JGP Journal of General Physiology

ARTICLE

Light drives the developmental progression of outer retinal function

Paul J. Bonezzi[1*], Matthew J. Tarchick[1*], Brittney D. Moore[1], and Jordan M. Renna[1]

The complex nature of rod and cone photoreceptors and the light-evoked responsivity of bipolar cells in the mature rodent retina have been well characterized. However, little is known about the emergent light-evoked response properties of the mouse retina and the role light plays in shaping these emergent responses. We have previously demonstrated that the outer retina is responsive to green light as early as postnatal day 8 (P8). Here, we characterize the progression of both photoreceptors (rods and cones) and bipolar cell responses during development and into adulthood using ex vivo electroretinogram recordings. Our data show that the majority of photoreceptor response at P8 originates from cones and that these outputs drive second-order bipolar cell responses as early as P9. We find that the magnitude of the photoresponse increases concurrently with each passing day of postnatal development and that many functional properties of these responses, as well as the relative rod/cone contributions to the total light-evoked response, are age dependent. We compare these responses at eye opening and maturity to age-matched animals raised in darkness and found that the absence of light diminishes emergent and mature cone-to-bipolar cell signaling. Furthermore, we found cone-evoked responses to be significantly slower in dark-reared retinas. Together, this work characterizes the developmental photoresponsivity of the mouse retina while highlighting the importance of properly timed sensory input for the maturation of the first visual system synapse.

Introduction

The establishment and subsequent refinement of early neural networks are crucial for proper visual function in mature organisms. In the developing mammalian visual system, a myriad of cues drives normal circuit formation, many of which depend largely on sensory experience. Several seminal studies have demonstrated the importance of light exposure during developmental critical periods on the formation of higher-order visual system circuitries (Hubel and Freeman, 1977; Hubel et al., 1977; LeVay et al., 1980; Huberman et al., 2008). These downstream cortical pathways both pool and filter incoming information from multiple levels of neuronal organization, making it difficult to isolate the root cause of circuit alterations in such cases of vast signaling interdependencies. Furthermore, light-dependent remodeling is thought to not only affect the visual cortex but has also been demonstrated to be required for intraretinal wiring. Numerous light-driven alterations occur in the developing retina, such as synaptic refinement at both the first retinal synapse in the outer plexiform layer (OPL; Dunn et al., 2013) and at the second synapse in the inner plexiform layer (IPL; Sosula and Glow, 1971; Fisher, 1979; Tian and Copenhagen, 2003). Furthermore, at bipolar cell axon terminals, active zones store and release neurotransmitter vesicles for rapid signaling. This activity alone shapes the normal patterns of synaptic connectivity during postnatal development (Kerschensteiner et al., 2009).

In mice, the visual system develops both pre- and postnatally, with eye opening occurring between postnatal day 12 (P12) and P14 and completing maturation around P30 (Olney, 1968; Fisher, 1979). Genetics and molecular cues drive much of the initial layout of the retina, beginning with the inner retina during early development and progressing outward to the photoreceptors closer to the time of eye opening (LaVail, 1973; Fisher, 1979; Rich et al., 1997; Sharma et al., 2003). Postnatal refinement of this initial layout, as well as the downstream, higher-order neuronal mappings, requires spatially and temporally correlated patterns of spontaneous activity across the inner retina, those of which are known as retinal waves (Meister et al., 1991; Wong, 1999). Cholinergic neurotransmission drives these waves from P0–P8, whereas glutamatergic transmission does so from P8 onward until eye opening when these waves disappear almost completely (Feller et al., 1996; Zhou and Zhao, 2000; Ford and Feller, 2012). Light input through intrinsically photosensitive ganglion

[1]Department of Biology, The University of Akron, Akron, OH, USA.

*Paul J. Bonezzi and Matthew J. Tarchick contributed equally to this paper. Correspondence to Jordan M. Renna: jrenna@uakron.edu.

cells (ipRGCs) can also modify and alter the temporal properties of this wave activity (Renna et al., 2011). Finally, around P10, it is likely that this spontaneous, inner retinal activity then intermingles with light-driven input from the outer retinal rod and cone photoreceptors (Tian et al., 2015).

Many studies have characterized the structural (LaVail, 1973; Blanks et al., 1974; Carter-Dawson and LaVail, 1979a; Carter-Dawson and LaVail, 1979b; Bodenstein and Sidman, 1987; Rich et al., 1997; Sharma et al., 2003) and functional (Luo and Yau, 2005; Heikkinen et al., 2008; Heikkinen et al., 2011; Heikkinen et al., 2012) development of these photoreceptors as the mouse begins to navigate its surroundings. Such studies have confirmed that the light-evoked photoresponse matures over the few weeks following eye opening and become stable by P30 (Luo and Yau, 2005; Heikkinen et al., 2012). By eye opening, many of the morphological features of the mouse retina, aside from the rod outer segments (OS) and specific synaptic connectivity in the OPL and IPL, are thought to parallel that of the mature retina. Indeed, much of the machinery required for cone phototransduction and synaptic signaling is present before P10 and completes a significant portion of their connectivity with postsynaptic partners by eye opening (Blanks et al., 1974; Rich et al., 1997; Fei, 2003; Sharma et al., 2003; Kim et al., 2008; Regus-Leidig et al., 2009; Aavani et al., 2017; Daum et al., 2017).

Synaptogenesis within the OPL between photoreceptors and bipolar cells begins at P7. This forms the initial bridge in signaling between the outer and inner retina. These connections continue maturing until the third postnatal week (Fisher, 1979; Johnson et al., 2003; Morgan et al., 2008). Even so, to our knowledge, there is no published evidence directly characterizing a single or populational bipolar cell response before eye opening in the mouse retina. We previously reported outer retinal photoresponsivity to bright (photopic) green light as early as P8 (Bonezzi et al., 2018). Here, we build on this study and characterize the developmental progression of populational photoreceptor (rod and cone), as well as ON bipolar cell responsivities, in normal-reared and dark-reared retinas to determine how developmental light input shapes responsivity across multiple information channels of the retina.

Materials and methods

Ethical approval

Experiments were conducted according to the National Institutes of Health guidelines. Animal use protocols were approved by the Institutional Animal Care and Use Committee at the University of Akron.

Animals

All experiments were conducted with both male and female C57BL/6R and *Gnat1*$^{-/-}$ (Calvert et al., 2000) mice (with littermate controls). We recorded from the retinas of mice at P8, P9, P10, and P14, as well as mice spanning 30–60 d of age for adult (mature) subjects. Normal-reared mice and *Gnat1*$^{-/-}$ were raised on a 12/12 h dark/light cycle and dark-reared mice were raised in 24 h of darkness and cared for under dim red (630 ± 20 nm) LED light (Roithner LaserTechnik). Animals had ad lib access to food and water. Mice were dark-adapted for at least 6–12 h before experiments. All experimental procedures were performed under dim red LED light and conducted between 10 am and 10 pm EST. Mice younger than P14 were sacrificed with 0.2 ml pentobarbital sodium (Fatal plus; Vortech Pharmaceuticals) while P14 and adult mice were sacrificed with CO_2 asphyxiation at the rate of 1.4–5.3 lpm. Both primary sacrificial methods were followed by cervical dislocation. Eyes were removed, placed on a cotton ball in a petri dish containing Locke's media supplemented with $BaCl_2$, and bubbled with 95% O_2 and 5% CO_2. Retinas were isolated from the eye, separated from the retinal pigmented epithelium layer (RPE), and prepared for recordings.

Electrophysiology

Transretinal, ex vivo ERGs were recorded from whole, intact mouse retinas with methods described previously (Bonezzi et al., 2020), using a recording chamber adapted from previous studies (Heikkinen et al., 2008; Vinberg and Kefalov, 2015). Electrode pairs (2× Ag/AgCl pellets housed in a 3-D printed component) provided signal detection. Locke's media bubbled with 95% O_2 and 5% CO_2 was preheated on a hot plate (VWR) and gravity fed (2–3 ml/min) through an inline heater (SH-27B; Sutter Instruments), and temperatures were monitored and maintained at (35–37°C) near the tissue with a thermocouple (TC-324C; Sutter Instruments). For a single experiment (n = 2 retinas), we first recorded ON bipolar cell–evoked b-waves in Locke's media supplemented with $BaCl_2$ (150 µM) to remove the slow (P-III), Müller cell component (Bolnick et al., 1979). We then isolated photoreceptor-driven a-waves by adding two glutamatergic agonists, L-AP4 (20 µM; Tocris) and L-aspartate (2 mM), to block the ON bipolar cell contributions to the ERG waveform (Murakami and Kaneko, 1966; Pepperberg et al., 1978; Heikkinen et al., 2008). We also chose to perfuse retinas with Locke's media over artificial cerebrospinal fluid or Ames' media since the hyperpolarization-activated "nose component" is typically more prominent this way, and assessing rod saturation was vital to many of our experiments (Vinberg et al., 2009; Heikkinen et al., 2012). All reagents were purchased from Sigma-Aldrich unless stated otherwise.

Data acquisition

ERGs were recorded with the positive terminal leads plugged into the bottom chamber (ganglion cell side) to prevent the need for response inversion during analysis. Because ERGs detect extracellular, transretinal voltages, conventional photoreceptor-evoked light responses appear positive-going when the positive terminal (recording) electrode is positioned contiguous with the photoreceptor side of the retina due to the hyperpolarizing nature of the rod and cone photoresponse. Before recordings, voltage offsets and resistances between the electrode pairs were measured to assure optimal recording conditions. DC signals were amplified ×1,000 (Multiclamp 700B; Molecular Devices), low-pass filtered (8-pole Bessel) at 300 Hz, digitized (Digidata 1550B; Molecular Devices) at 10 kHz, and stored on the computer (7620; Dell Precision). Both recording and light stimulus protocols were set within acquisition software (Clampex 10.0; Molecular Devices).

Light sources, calibrations, and tissue stimulation

The 4× microscope objective (BX51WI; Olympus) provided short, full-field (1–10 ms) flashes to the photoreceptor side of the retina from an LED (X-Cite 120 LED; Lumen Dynamics) driven by TTL signals configured by a computer. Dichroic filter cubes (ET-DAPI HYB and C170479; Chroma) and neutral density filters (22000; Edmund Optics) placed in the light path controlled the incident photon density and initial wavelength. Because the spectral sensitivities of m-opsin and s-opsin overlap by a considerable degree, we used a bandpass filter (520 ± 23 nm; 86984; Edmund Optics) to primarily drive m-opsin cone pigment. The overlap in spectral sensitivities of m-opsin with that of s-opsin (~20% λ_{max}; Govardovskii et al., 2000) means that a given response may have contained both s-opsin- and m-opsin-driven activity, which is unavoidable aside from separating and recording from each half of the retina individually. However, we recorded from intact retinas with hopes of maximizing response robustness from immature tissue, and thereby avoided attempts to separate m/s-opsin-driven responses by using specific portions of the retina (Lyubarsky et al., 1999; Applebury et al., 2000; Nikonov et al., 2006). Microscope apertures were adjusted so that a 10-mm Ø light spot stimulated both retinas simultaneously. For separation of rod and cone light responses, digitizer signals configured within acquisition software (Clampex 10.0; Molecular Devices) drove monochromatic (505 ± 10 nm) LEDs (B5-433-B505; Roithner LaserTechnik) housed in a 3-D-printed objective adapter (Bonezzi et al., 2020), providing steady background light to saturate the rods.

Light sources were calibrated with an optometer (S470 flexOptometer, Gamma Scientific) and a photodiode probe (260M/7K001; Gamma Scientific) measuring W cm^{-2} which were then converted to photons per cm^2. Estimations of flash-evoked photoisomerizations per rod or cone cell were achieved considering the following: the light sources' emission spectrum, the photoreceptors' OS dimensions (LaVail, 1973; Carter-Dawson and LaVail, 1979a; Nunn et al., 1984), the absorption spectrum of the cells' opsin(s) (rhodopsin, rod-dominant opsin, λ_{max} = 498 nm; s-opsin, s-cone dominant opsin, λ_{max} = 361 nm; m-opsin, m-cone dominant opsin, λ_{max} = 508 nm; Lyubarsky et al., 1999; Applebury et al., 2000; Govardovskii et al., 2000; Yokoyama, 2000), and a particular stimulation geometry (Heikkinen et al., 2008; Heikkinen et al., 2011; Vinberg et al., 2014). Collectively, these provided an estimate of a single photoreceptor's collecting area (a_c; μm^{-2}) and permitted calculations of photoisomerizations from the flash intensity I (photons μm^{-2}) with the following equation:

$$\phi = I_{h\nu}.a_c. \quad (1)$$

For adult animals (≥30 d), calculations of a_c were based on known dimensions of mature rod and cone photoreceptors (Carter-Dawson and LaVail, 1979a). For developmental animals (P8–P14), rod and cone outer segment dimensions were obtained from previous morphological analyses (LaVail, 1973; Obata and Usukura, 1992; Daum et al., 2017) and used for estimations of a_c, taking into consideration the dimensions (length × diameter) of the emerging OS of cones (P8; 3 × 1.4 µm) and rods (P8; 0.5 × 0.8 µm), of which cones reach near-mature OS volume by eye opening (P14; 13.4 × 1.4 µm) and rods between P21 and P22 (P30; 24 × 1.4 µm). With these dimensions, we were able to calculate the a_c using the following equation as seen in Baylor et al. (1984):

$$a_c = f\frac{\pi d^2}{4}\left[1 - 10^{-\Delta D(\lambda) l}\right]\gamma, \quad (2)$$

where f is the factor that accounts for light funneling by the inner segment, γ is the quantum efficiency of photoisomerization, and d and l are the diameter and length of the outer segments, respectively. Because we stimulated tissue from the photoreceptor side of the retina, the funneling effect from the rod's inner segments is negligible (f = 1). $\Delta D(\lambda)$ is the specific density of the outer segment at wavelength λ. The specific density of the outer segments at λ_{max} the value for $\Delta D(\lambda)$ = 0.016 (Nymark et al., 2005) and γ = 2/3. From the pigment template, we get ΔD(520 nm) = 0.86 $\Delta D(\lambda_{max})$ for the mouse rods (λ_{max} = 498 nm; Lyubarsky et al., 1999), and we arrive at $a_{c,\mathrm{rod}}$(520 nm) = 0.55 μm^{-2} for adult rods with our stimulus wavelength. This same calculation was performed for rods and cones at younger postnatal ages considering the OS dimensions.

Therefore, estimated total a_c (rods + cones) under mesopic flashes for P8–P10 retinas are as follows for 520 nm flashes: P8 = 0.036 μm^2; P9 = 0.066 μm^2; and P10 = 0.088 μm^2. Due to uncertainties in these estimations, as well as the abnormally high (A) values when calculated in terms of (P*), we report light stimulus values as photons per μm^2 and amplification constants (A) in terms of both photoisomerizations rod^{-1} s^{-1} (P*) as well as photons per μm^2 (Table 1).

Separation of rod and cone responses

To isolate cone responses, we used two different methods. We took advantage of a rod's high sensitivity to photons compared with that of cones (see Ingram et al, 2016). This method could be reliably used on animals at ages P10 and P14. However, because of the lower light sensitivity of photoreceptors at P8, we instead utilized *Gnat1*$^{-/-}$ animals. To accomplish background saturation, we superimposed mesopic–photopic flashes (1–10 ms) over a rod-saturating background (Fig. 1). This background elicited a substantial nose component indicative of rod saturation (Heikkinen et al., 2008; Vinberg et al., 2009; Vinberg et al., 2014) while minimally driving cones (Nikonov et al., 2006; Heikkinen et al., 2012). We avoided prolonged background light to prevent excessive pigment bleaching and alterations of responsivity through gap junctional coupling (Hornstein et al., 2005; Heikkinen et al., 2011; Asteriti et al., 2014; Ingram et al., 2019). The interstimulus interval was 500 ms for measuring a-waves and 1–1.5 s when measuring b-waves; this ensured that the initial rod-dominant b-wave reached a steady state before recording cone-evoked events (Heikkinen et al., 2008; Heikkinen et al., 2012; Kolesnikov and Kefalov, 2012; Vinberg et al., 2017). The inter-recording interval was 30 s for dim flashes and 90 s for saturating flashes in rod studies and 30 s for cones as their responses recovered rapidly even after bright flashes. We considered the possibility that the angled nature (15.2°) of this background could result in incomplete suppression of rod-circulating current (Stiles and Crawford, 1933; Matsumoto et al., 2012). However, this background was

Table 1. **ERG response properties from isolated retinas across postnatal development of normal-reared (nr) and dark-reared (dr) animals**

			A-waves									B-waves		
			Dim flash response properties					(hv µm²)	(P*)	STF				
Condition	**Contribution**	***n***	**R_{max} (µV)**	**R_{dim} (µV)**	**t_{peak} (ms)**	**τ_{rec} (ms)**	**t_{int} (ms)**	***$I_{1/2}$* (hv µm^{-2})**	***A* (s^{-2})**	***A* (s^{-2})**	***$A_{1/2}$* (µV)**	***n***	**R_{max} (µV)**	***$I_{1/2}$* (hv µm^{-2})**
P8 (nr)	Rods/cones	10	7 ± 0.7	4.1 ± 0.3	59 ± 6.8	751 ± 145	195 ± 15	921 ± 2,413	16 ± 4.5	135 ± 39	–	–	–	–
P8 *Gnat1*$^{-/-}$	Cones	4	2.7 ± 1.1	0.9 ± 0.3	306.5 ± 153.3	82.1 ± 30.9	257.3 ± 30.4	30,531.8 ± 22,646	–	–	–	–	–	–
P9 (nr)	Rods/cones	8	14 ± 2.9	4.8 0.5	116 ± 24	271.45 ± 43	178 ± 23	408 ± 335	6.7 ± 1.8	44 ± 12	–	6	–	–
P10 (nr)	Rods/cones	12	61 ± 11	13 ± 2.4	147 ± 17	206 ± 26	234 ± 20	55 ± 12	20 ± 3.4	96 ± 16	–	6	90 ± 52	27 ± 12
P10 (nr)	Cones	5	5 ± 1.4	5.2 ± 1.1	43 ± 4.5	129 ± 34	146 ± 29	10,402 ± 2,578	0.024 ± 0.005	0.31 ± 0.06	–	3	10 ± 3.1	12,711 ± 1,835
P10 *Gnat1*$^{-/-}$	Cones	16	13.9 ± 4.7	4.1 ± 1.5	332.3 ± 45.7	257.3 ± 89.6	302.1 ± 21.5	27,841 ± 18,600	–	–	–	–	–	–
P14 (nr)	Rods	12	258 ± 21	46 ± 10	177 ± 20	183 ± 20	204 ± 17	183 ± 12	16 ± 5.7	48 ± 17	17.1 ± 2.6	12	754 ± 58	6 ± 3.0
P14 (dr)	Rods	12	216 ± 45	56 ± 10	222 ± 22	228 ± 28	301 ± 34	145 ± 16	22 ± 5.0	69 ± 15	32.9 ± 9.2	12	743 ± 71	6 ± 2.8
P14 (nr)	Cones	12	28 ± 3.0	9.1 ± 8.8	68 ± 4.5	68 ± 0.3	60 ± 16	11,229 ± 494	0.6 ± 0.1	7.3 ± 1.6	23.2 ± 3.2	12	110 ± 8.9	16,625 ± 2,382
P14 *Gnat1*$^{-/-}$	Cones	11	14.6 ± 3.7	4.1 ± 1.3	296.5 ± 55.8	980.7 ± 565.6	370.4 ± 35.2	7,023 ± 2,577	–	–	–	–	–	–
P14 (dr)	Cones	11	34 ± 3.4	11 ± 1.2	64 ± 3.4	65 ± 8.9	64 ± 3.4	10,321 ± 752	0.9 ± 0.2	12 ± 3.2	26.1 ± 8.0	11	65 ± 6.8	8,903 ± 1,457
Adult (nr)	Rods	14	368 ± 23	77 ± 8.7	237 ± 16	269 ± 31	351 ± 30	186 ± 8.1	7.5 ± 1.3	14 ± 2.4	7.4 ± 2.7	10	1,719 ± 189	13 ± 2.9
Adult (dr)	Rods	14	381 ± 23	80 ± 28	196 ± 13	236 ± 56	293 ± 23	151 ± 7.4	10 ± 2.4	19 ± 4.4	4.0 ± 1.5	14	1,864 ± 92	15 ± 5.3
Adult (nr)	Cones	10	49 ± 6.1	18 ± 2.6	64 ± 2.4	61 ± 0.2	94 ± 14	13,328 ± 914	0.7 ± 0.3	9.4 ± 3.7	15.7 ± 4.1	7	269 ± 31	33,447 ± 5,935
Adult *Gnat1*$^{-/-}$	Cones	7	37.2 ± 4.5	11.7 ± 1.9	147.0 ± 17.9	205.9 ± 42.4	284.8 ± 19.9	10,474 ± 5,105	–	–	–	–	–	–
Adult (dr)	Cones	16	39 ± 3.7	9.2 ± 2.8	90 ± 7.8	97 ± 14	118 ± 10	73,800 ± 17,295	0.2 ± 0.03	2.1 ± 0.4	33.3 ± 3.7	18	78 ± 8	24,003 ± 2,979

All values represent the mean ± SEM. Non-applicable parameter measurements and parameters not measured are represented by –.

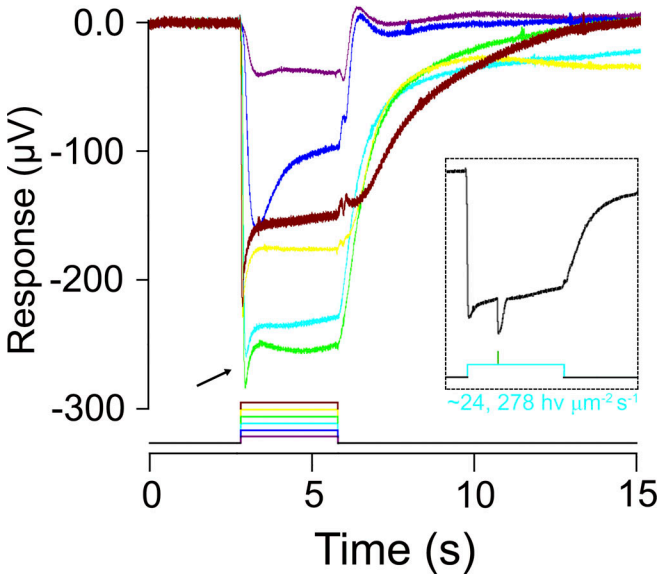

Figure 1. **Cone-driven flash responses isolated with ex vivo ERGs.** Ex vivo ERG recordings from a WT adult mouse retina demonstrate the use of background light for isolating cone-evoked responses from the rod-dominated ERG. Constant (3 s) 505 nm light steps of increasing intensity (square steps) were delivered between 98 (maroon trace) and 150,526 photons μm^{-2} s^{-1} (brown trace). The background light step delivering 24,278 photons μm^{-2} s^{-1} (cyan trace) most effectively suppressed rod-evoked activity while minimizing response run-down and light adaptation between trials (inter-recording interval = 60 s). The extended time scale illustrates the slowed response recovery to the offset of background steps of increasing intensity. Arrow indicates the nose component and subsequent steady-state response reflecting prolonged rod response suppression (see Materials and methods). Inset: Cone-mediated photovoltages isolated by superimposed flashes (1–8 ms) of 520 nm light over steady background illumination (interstimulus interval = 500 ms). This stimulus protocol was used for measuring all cone-driven responses throughout this study aside from those collected from *Gnat1*$^{-/-}$ retinas.

considerably stronger than those used in previous studies (24,278 photons μm^{-2} s^{-1} compared with 15,000–20,000 photons μm^{-2} s^{-1}), making it unlikely that a significant portion of the rod's dark current remained as responses routinely exhibited a nose component, indicative of saturation (Fig. 1; Heikkinen et al., 2008; Vinberg et al., 2009; Heikkinen et al., 2011; Heikkinen et al., 2012).

Using *Gnat1*$^{-/-}$ to separate rods and cones

A standard method to separate the contribution of cone responses from rod responses in ERGs is to use high background illumination to saturate the rod responses, leaving only a cone response intact. However, as rods develop, saturation of the rod photoresponse occurs at increasingly high intensities, such that, at particular developmental time points, a residual rod contribution may contaminate the ERG signal, i.e., some rods may not saturate (Tikidji-Hamburyan et al., 2017). To better isolate cone responses at different developmental time points, we take advantage of the fact that the rods and cone utilize different transducin isoforms. Transducin α-1 (*Gnat1*) is expressed in rods and transducin α-2 (*Gnat2*) is expressed in cones (Ingram et al. 2016). Genetic knockouts of the rod transducin, *Gnat1*$^{-/-}$ demonstrates a shift in intensity response function consistent with the presence of only intact cone function. Rods in the *Gnat1*$^{-/-}$ animals were not responsive to light in suction electrode experiments. The *Gnat1*$^{-/-}$ also is ideal for experiments that examine developmental changes in cone photosensitivity because the early morphology of the retina is not altered in the *Gnat1*$^{-/-}$ as it can be in other rod-silencing mutations (Calvert et al., 2000). Because of the lower light sensitivity of photoreceptors at early developmental ages, we utilized *Gnat1*$^{-/-}$ animals to exclude the possible contribution of rod photoreceptors at the early time points.

Data analysis

All analyses were performed before digital filtering. Representative response traces were digitally filtered at 40 Hz. Peak analyses were performed in Clampfit 10.0. The a-wave amplitudes for both rods and cones recorded with no pharmacological blockers were measured as the negative-going local minimum after light stimulus onset (time = 0 s). In the presence of pharmacological blockers, a-wave amplitudes were measured from the negative-going, saturated response plateau after the sharp nose component, for rod recordings, and simply as the peak amplitude from cone recordings. To determine retinal sensitivity, half-saturation and cooperativity parameters ($I_{1/2}$ and n) were derived from best-fitting intensity response relationships of both a- and b-waves with the Hill-type fitting equation:

$$\frac{R}{R_{max}} = \frac{I^n}{\left(I_{1/2}^n + I^n\right)}, \quad (3)$$

where R is the response at flash intensity (I), R_{max} is the saturated response for a single retina elicited by a flash intensity (I), $I_{1/2}$ is the flash intensity required to elicit half of R_{max}, and n is the cooperativity parameter determined by the fitting function. For rod b-waves, R_{max} was determined as the amplitude prior to the onset of the secondary linear growth phase in the fit after the sigmoidal behavior. The t_{peak} (time-to-peak) for both rods and cones was calculated as the time (in ms) of the local minimum after stimulus onset of the dim flash response (R_{dim} = 20–30% R_{max}). The t_{int} (integration time; ms) for both rods and cones was determined as the integral of the dim flash response (μV.ms) divided by the dim flash response amplitude (R_{dim}; μV). The recovery time constant (τ_{rec}) was determined by normalizing R_{dim} or 70–80% R_{max} to their peak and then fitting the response recovery (peak to V_o) with a single exponential:

$$R = V_o exp^{\frac{-t}{\tau}}. \quad (4)$$

To determine the dominant time constant (τ_D) of rod response recovery, we applied a Pepperberg analysis (Pepperberg et al., 1992). We first plotted the time required (in s) for 40% recovery from R_{max} (quantified as the flattest point in the saturated plateau region following the nose component) against the log of stimulus intensities (photons μm^{-2}). We then applied a linear fit to the first three saturated responses to obtain the dominant time constant. For determination of phototransduction activation rates, amplification constant A (s^{-2}) from the first three to five most dim, averaged, and normalized traces,

were fit to the first one-third to one-half of the rising phase with a modified version of the LP model of phototransduction (Lamb and Pugh, 1992; Pugh and Lamb, 1993) given by the equation:

$$\frac{R}{R_{max}} = \left(1 - e^{\left(-a\left(t-t_{eff}\right)^2\right)}\right), \quad (5)$$

where t_{eff} represents a short delay (effective time delay) between the stimulus onset and response onset. The parameter, (a), was then multiplied by 2 and divided by the effective photons used in that trial for the determination of (A) in terms of effective photons per μm². For the determination of (A), in terms of activated pigment molecules (P*), (a) was instead divided by the collecting area of rods and/or cones depending on the experiment (a_c).

To determine how effectively photoreceptors drive second-order bipolar cells across the photoreceptors' dynamic range, we calculated ratios of b-waves and a-waves at given flash intensities. Ratios of b-wave and a-wave amplitudes were calculated by dividing the b-wave by the a-wave in single traces treated with $BaCl_2$, in the absence of b-wave blockers, and subsequently averaged across identical flash intensities. For this measurement, b-wave amplitudes were calculated from the baseline to the positive-going peak while a-waves were measured from baseline to the negative-going trough.

Furthermore, to determine the sensitivity of bipolar cells to photoreceptor output in a stimulus-intensity agnostic manner, we then generated the synaptic transfer function for individual retinas. To obtain the a-wave amplitude required to half-maximally drive the b-wave, the synaptic transfer function was fit with a Hill-type function using the equation:

$$\frac{R_B}{Rmax_B} = \frac{R_A^n}{k^n + R_A^n}, \quad (6)$$

where R_B is the response of the b-wave and $Rmax_B$ is the highest b-wave response in a single retina elicited by an a-wave (R_A). The semi-saturation constant (k) is the a-wave response required to elicit half of the $Rmax_B$ and (n) is the cooperativity parameter determined by the fitting function.

Fitting, statistics, and custom Julia code

All fitting was performed in Originlabs 2020 (OriginLab). Data are presented as mean ± SEM. A Student's t test was used for unpaired data, and two-way ANOVA was used to compare response parameters across all conditions (postnatal age and rearing condition). Statistical significance was set at $P < 0.05$ (Graphpad-Prism). A/B-wave ratios and synaptic transfer functions were fit using custom-written Julia software available at https://github.com/mattar13/ElectroPhysiology.jl.

Results

Previous studies from mouse retina have described the physiological function of rods, cones, and bipolar cells at the time of, or after eye opening. Although these studies have laid the groundwork for understanding the complex nature of mature photoreceptor and bipolar cell function, little is known about the light-evoked response properties of such cells across early postnatal development of the mouse retina. We have previously demonstrated that the outer retina is responsive to green light (561 nm) as early as P8 (Bonezzi et al., 2018). Here, we build on these original findings by first starting from the earliest time point in postnatal development in which we were able to detect light responses. Furthermore, because little was known about how environmental light exposure drives normal cellular activities and functional wiring in the outer retina, we compare these responses at eye opening and maturity to age-matched animals raised in darkness.

The progression of retinal photoresponsivity from threshold to maturation

To probe the photoresponsivity of the mouse retina across early postnatal development, we began by conducting transretinal, ex vivo ERGs from P8–P10 animals (Fig. 2 A). In the absence of rod-suppressing background light, saturated a-wave amplitudes (R_{max}) increased proportionally with age in both WT and *Gnat1*$^{-/-}$ animals (Fig. 2 and Table 1), paralleling the increased sensitivity at each age (Fig. 2 B). Considering the already-low sensitivity of the retina at P8 and P9, we were incapable of isolating cone-dominated responses in the presence of a rod-saturating background until P10 (Fig. 2 A, inset). Because of this challenge, and the uncertainty of the effectiveness of the use of background light on developing retinas, early postnatal recordings were also made from *Gnat1*$^{-/-}$ retinas (Fig. 2 A).

A few key factors indicate that rod and cone functions exhibit distinct developmental time scales. We detected similarly sized a-waves at P8 (Fig. 2 A) from WT and *Gnat1*$^{-/-}$ animals, indicating this time point represents the developmental onset of cone-driven activity. Compared with other ages, responses at P8 exhibited lower sensitivity and quickly reached saturation after only a 2-log unit increase in light intensity (Fig. 2 B), therefore, exhibiting an extremely compact dynamic range. Subsequently, in P9 WT retinas, a small nose component became evident indicating the emergence of rod-driven activity (Fig. 2 A, black arrow; Vinberg et al., 2009; Robson and Frishman, 2014; Van Hook et al., 2019). Lastly, sensitivity was a full log unit greater at P10 than at P9 between WT and *Gnat1*$^{-/-}$ (Fig. 2 B). From P8 to P10, WT responses roughly doubled in amplitude after each day of development while concurrently increasing in sensitivity by 1 log unit (Fig. 2 B). However, for *Gnat1*$^{-/-}$ retinas, the sensitivity and R_{max} also increased with age but reached relatively larger amplitudes earlier in development than WT retinas (Table 1). Collectively, these results highlight key aspects of outer retinal sensitivity before eye opening: cone responses emerge at P8, the dynamic range of the retina is compact (~2 log units of photons μm^{-2}) from P8–P9, rod-driven activity emerges at P9, and both rods and cones contribute similar proportions to the ERG at P10.

To further characterize the developmental progression of retinal photoresponses, we made recordings at two additional age points, eye opening (P14) and adulthood (>P30; Fig. 2, C and D). In mature WT retinas, maximal b-wave amplitudes increased from those at eye opening by about 50% (adult: $n = 10$; P14: $n = 12$, $P = 0.0008$) and retinal sensitivity also increased significantly (adult: $n = 10$; P14: $n = 12$, $P = 0.008$). Likewise, maximal a-waves

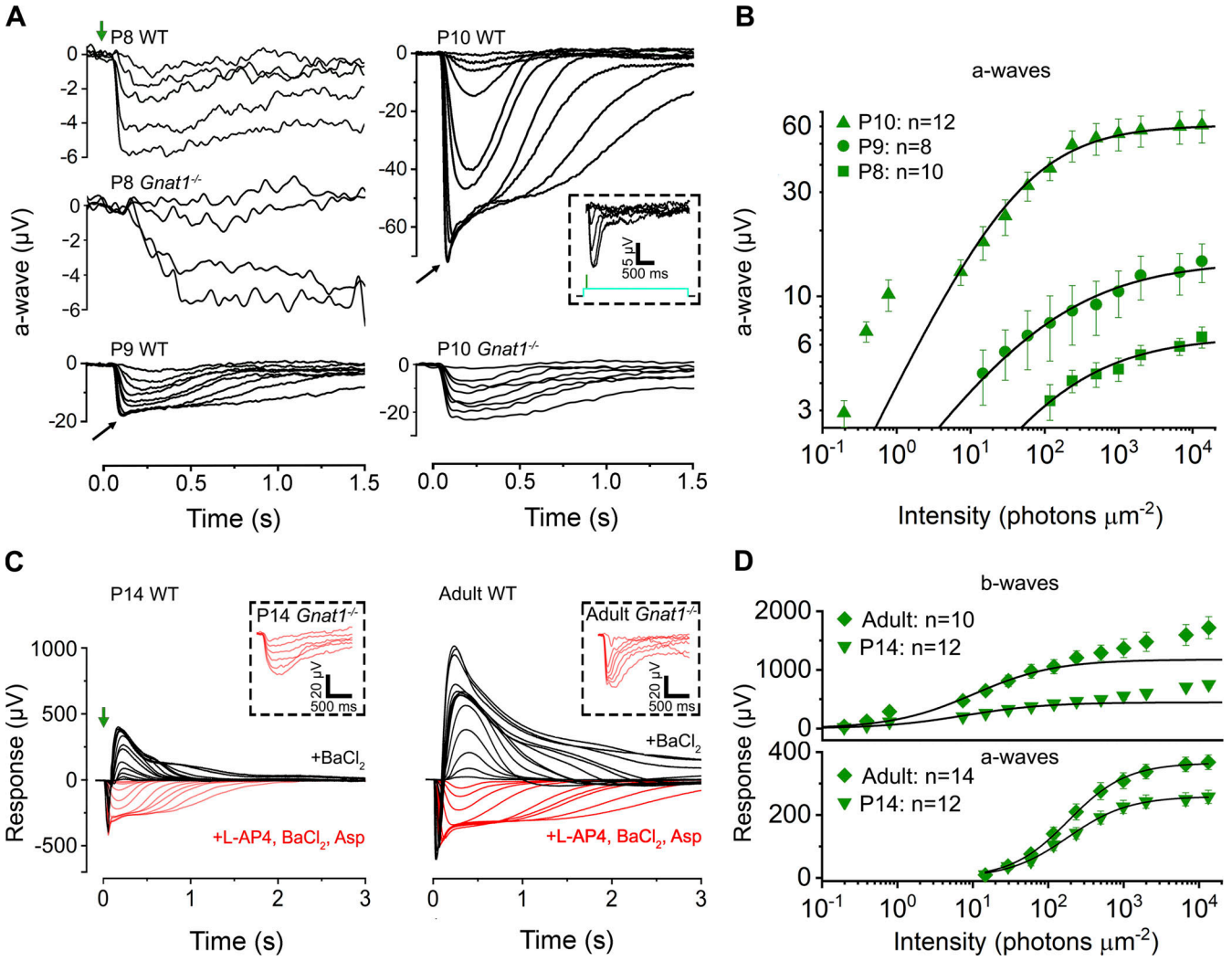

Figure 2. **Rod and cone contributions to the ERG depend on postnatal age.** The developmental progression of the mouse ERG. **(A)** Both WT and *Gnat1*$^{-/-}$ photoreceptor responses emerge at P8 and increase rapidly in amplitude thereafter. Photoreceptor-driven a-waves at P8, P9, and P10 evoked by green (520 nm) flashes of increasing intensity (delivering 0.19–13,280 photons μm^{-2}) presented at t = 0 (green arrow). Cone responses obtained from *Gnat1*$^{-/-}$ animals were evoked by the light of increasing intensity (delivering 379–83,835 photons μm^{-2}) without background saturation. The rod-driven nose component emerges at P9 (black arrow) and becomes more robust at P10. Inset: Cone-evoked responses at P10 isolated under the stimulus protocol from Fig. 1. **(B)** In emergent time points, the dynamic range of the retina is compact at P8. This remains consistent until adulthood. The sensitivity, however, increases by ∼1 log unit with each passing day in development. Population averaged a-wave amplitudes plotted as a function of flash intensity, from P10 (triangle, n = 12), P9 (circle, n = 8), and P8 (square, n = 10) retinas. **(C)** Outer retinal signaling increases at a slower rate between eye opening and maturity. Response families to the same stimuli used in A from P14 (left) and adult (right) retinas. Insets represent *Gnat1*$^{-/-}$ a-waves at corresponding time points without background saturation. Retinas were initially perfused with Locke's media containing $BaCl_2$ to observe both the negative-going photoreceptor component and the positive-going bipolar cell-driven components, then subsequently with additional blockers (see Materials and methods) to isolate the photoreceptor-driven a-wave (red traces). **(D)** Retinal sensitivity increases at a slower rate (50–60%) between eye opening and adulthood. Population averaged b-wave (top) and a-wave (bottom) amplitudes plotted as a function of flash intensity in P14 (inverted triangle, n = 12 and 16) and adult (diamond, n = 10) retinas. Black fit lines = best fit of Eq. 2. Resultant $I_{1/2}$ values are listed in Table 1. Error bars = mean ± SEM.

increased by 65% (adult: n = 14; P14: n = 12, P < 0.0001). The increase in a-waves indicates a much slower growth rate when compared on a day-by-day basis with of those a-waves recorded from retinas before eye opening. To characterize cone-mediated activity at these two ages, we then isolated a-waves from *Gnat1*$^{-/-}$ retinas (Fig. 2 C, insets), finding that the cone-driven a-wave grows by ∼40%, similar to that of the rod-driven a-wave in WT mice (adult: n = 7; P14: n = 11).

Compared with all ages, adult WT retinas were most sensitive, and it was at this point in development that sensitivity stabilized for both ON bipolar cells and photoreceptors (Fig. 2 D). Despite the increasing sensitivity, the dynamic range was still maintained at ∼2 log units of photon intensity in both a- and b-waves. As flash stimuli were within the scotopic–mesopic range and presented in the absence of background light, we presume the WT adult responses to be predominately rod-driven. In agreement with previous ERG studies, both P14 and adult WT rod-driven a-waves exhibited a strong nose component upon saturation while those of *Gnat1*$^{-/-}$ retinas did not (Fig. 2 C). Overall, these data are consistent with previous

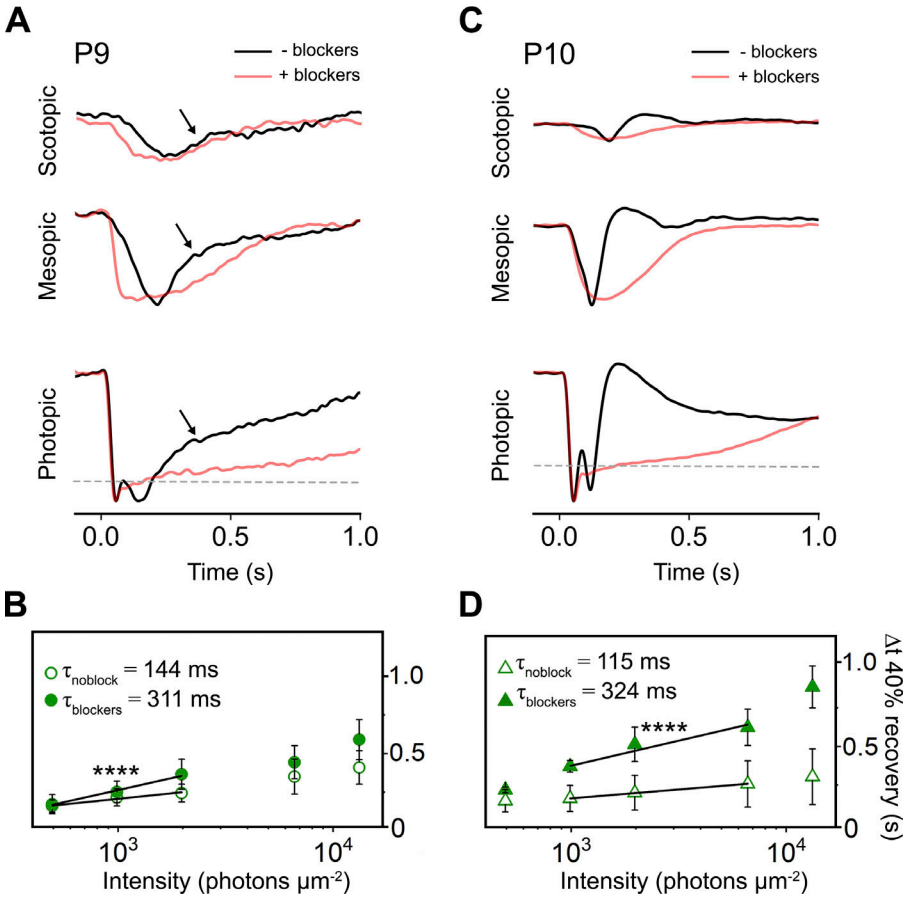

Figure 3. **Scotopic responses and bipolar cell-mediated activity emerge at P9.** Emergent bipolar cell activity shapes the ERG waveform at P9 and P10. **(A and C)** Normalized a-waves from P9 (A) and P10 (C) retinas to short (1–10 ms) green flashes presented at t = 0 s. Flashes delivering 0.19–117 photons μm^{-2} elicited scotopic responses (first row), 234–495 photons μm^{-2} elicited mesopic responses (second row), and those flashes delivering 13,280 photons μm^{-2} elicited photopic responses (bottom row). Synaptic blockers (see Materials and methods) were then perfused to eliminate any bipolar cell contribution, and subsequent recordings were repeated in the same retinas using identical flashes (red traces). Arrows in A represent a positive going pull on the waveform. **(B and D)** A Pepperberg analysis (see Materials and methods) on P9 (B) and P10 (D) data reveal the effect of bipolar cell-mediated activity on the waveform. Response recovery time (Δt to 40% recovery after the emerging nose component—dashed horizontal line) to the five brightest green flashes used in Fig. 2, plotted as a function of the first three (P9) and the middle three (P10) brightest flash intensities. The dominant time constant of recovery (τ_D) was significantly greater in retinas perfused with blockers (P9: n = 5 and 6, P = 2.6789 × 10^{-5} and became more obvious at P10 (P10: n = 10 and 9, P = 7.0149 × 10^{-11}). Error bars = mean ± SEM. Asterisks indicate a P value of <0.001.

reports of mature rod photoresponses measured with ERGs (Heikkinen et al., 2008; Heikkinen et al., 2012; Vinberg and Kefalov, 2015).

Bipolar cell-mediated activity and scotopic threshold emerges at P9

To gain insight into the emergence of bipolar cell-driven activity, we conducted additional recordings on WT P9 and P10 retinas in the absence, and subsequently in the presence of synaptic blockers, like recordings seen in Fig. 2 C.

At P9, dim flashes elicited photoreceptor-mediated a-waves, marking the onset of detectable scotopic activity (Fig. 3 A, black trace). Interestingly, when comparing the P9 responses without b-wave blockers to those with blockers, we noticed that, depending on the flash intensity, responses exhibited a shift to their activation phase and/or their recovery phase. In response to scotopic–mesopic flashes, a positive-going "pull" on the waveform delayed the activation phase and shortened the recovery phase of the response (Fig. 3 A, arrows). However, at photopic intensities, the activation phase was no longer delayed, while the recovery phase was affected by the same pull. Although an unconventional use case, we performed a Pepperberg analysis (see Matrials and methods) to determine if this pull reduced the dominant time constant.

It was determined that the dominant time constant (τ_D) of the saturated response recovery was shorter in the absence of blockers compared to that with blockers (n = 5 and 6, P = 2.6789 × 10^{-5}; $\tau_{noblock}$ = 144 ± 23; τ_{block} = 311 ± 36 ms; Fig. 3 B), indicating that this pull in the waveform was in fact sufficient to shorten the apparent time under saturation. This phenomenon was also present at P10 (n = 10 and 9, P = 7.0149 × 10^{-11}, $\tau_{noblock}$ = 115 ± 4 ms; τ_{block} = 324 ± 61 ms; Fig. 3 D). Furthermore, in the presence of blockers, responses at P10 were slower to recover, suggesting an increasing rod contribution to the total photovoltage further into development. We presume this pulling effect to be an emergent, ON bipolar cell-driven activity, shaping what we have termed the "b-wave threshold response" (BTR). However, it remains unclear to what degree this b-wave is rod- or cone-mediated. This tendency unveils a competing nature of photoreceptor and ON bipolar cell contributions to the immature waveform. However, at P10, the scotopic responses were more robust, generating a b-wave with a traditional positive-going component that out-measured the negative-going a-wave as it crossed baseline (Fig. 3 C). In summary, both scotopic (rod) threshold and bipolar cell-mediated activity emerge 1 d after cone responses appear.

Functional properties of photoreceptor responses are age dependent

Next, to further characterize the nuances of photoreceptor-evoked activity we begin by plotting the normalized (R/R_{max}) dim flash responses from isolated a-waves across development (Fig. 4 A). From these dim flash responses, we measured several metrics of waveform kinetics including time-to-peak (t_{peak};

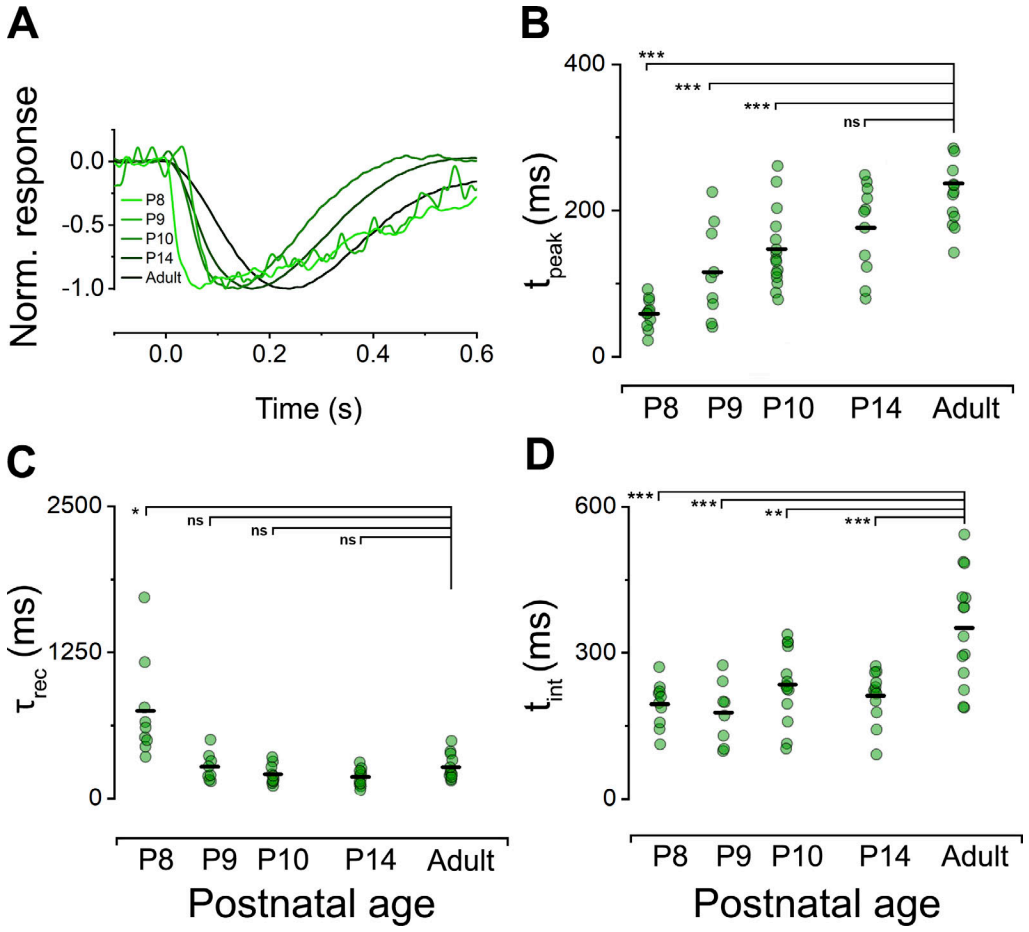

Figure 4. **Response kinetics of the rod-dominated ERG are age-dependent.** Rod-dominant a-wave properties of P8, P9, P10, P14, and adult retinas in response to dim flashes. **(A)** Representative a-wave traces normalized to their peaks illustrate an age-dependent shift in waveform kinetics. **(B–D)** Dim flash response properties of individual retinas (green circles; n = 1) plotted across postnatal age. After P9, t_{peak} (B) decreases significantly with decreasing postnatal age when compared with adult (adult: n = 14, 237 ± 16 ms; P14: n = 12, P = 0.1617 [n.s.], 177 ± 20 ms; P10: n = 12, P = 6.832×10^{-4} [***], 147 ± 17 ms; P9: n = 8, P = 4.71×10^{-5} [***], 115 ± 24 ms; P8: n = 10, P = 4.11×10^{-11} [***], 59 ± 6.8 ms). **(C)** When compared with adult animals, only P8 retinas displayed a longer recovery time constant (τ_{rec}; see Eq. 3) compared with all other ages (adult: n = 14, 269 ± 31 ms; P14: n = 12, P = 0.999 [n.s.], 183 ± 20 ms; P10: n = 12, P = 0.999 [n.s.], 206 ± 26 ms; P9: n = 8, P = 0.999 [n.s.], 271 ± 14 ms; P8: n = 10, P = 0.0163 [*], 751 ± 145 ms). **(D)** Conversely, integration time (t_{int}) was exclusively extended at maturity compared to all other ages (adult: n = 14, 269 ± 31 ms; P14: n = 12, P = 0.00011, 183 ± 20 ms; P10: n = 12, P = 0.0015, 206 ± 26 ms; P9: n = 8, P = 1.3407×10^{-5}, 271 ± 43 ms; P8: n = 10, P = 3.1630×10^{-5}, 195 ± 15 ms). Black bars represent the population means. Single, double, and triple asterisks indicate a P value of <0.05, <0.01, and <0.001, respectively.

Fig. 4 B), recovery time constant (τ_{rec}; Fig. 4 C), and integration time (t_{int}; Fig. 4 D). Additionally, to gain insight into any age-dependent requirements on the activation phase of phototransduction, we approximate amplification rates from the rising phase of the a-wave across several light intensities. The values associated with these response properties are also listed in Table 1.

First, aside from P14 responses, the t_{peak} was notably shorter in younger animals (adult: n = 14, 237 ± 16 ms; P14: n = 12, P = 0.1617 [n.s.], 177 ± 20 ms; P10: n = 12, P = 6.832×10^{-4} [***], 147 ± 17 ms; P9: n = 8, P = 4.71×10^{-5} [***], 115 ± 24 ms; P8: n = 10, P = 4.11×10^{-11} [***], 59 ± 6.8 ms; Fig. 4 B). Notably, the t_{peak} at P8 (59 ± 6.8 ms) reflected that of previously published cone-driven ERGs (Heikkinen et al., 2008; Heikkinen et al., 2012). We also estimated amplification constants (A) at each age and noticed a similar trend as the t_{peak} values. In the absence of background light, the amplification rate of phototransduction reflected more closely to that of rods than that of cones in recordings from mature tissue. However, as rod amplification constants calculated in terms of photoisomerizations rod^{-1} (P^*), seemed considerably higher than normal, we also present these values in terms of effective incident photons (photons μm^{-2}). The recovery time constant (τ_{rec}) did not differ significantly from adulthood at any other age than P8 (adult: n = 14, 269 ± 31 ms; P14: n = 12, P = 0.999 [n.s.], 183 ± 20 ms; P10: n = 12, P = 0.999 [n.s.], 206 ± 26 ms; P9: n = 8, P = 0.999 [n.s.], 271 ± 14 ms; P8: n = 10, P = 0.0163 [*], 751 ± 145 ms; Fig. 4 C). Lastly, the integration time (t_{int}) was significantly longer in adulthood compared with any other age (adult: n = 14, 269 ± 31 ms; P14: n = 12, P = 0.00011, 183 ± 20 ms; P10: n = 12, P = 0.0015, 206 ± 26 ms; P9: n = 8, P = 1.3407×10^{-5}, 271 ± 43 ms; P8: n = 10, P = 3.1630×10^{-5}, 195 ± 15 ms; Fig. 4 D). Considering these analyses, it appears that before P10, the mouse ERG contains both cone and rod-driven contributions and becomes increasingly rod-dominated into adulthood.

Normal photoreceptor signaling requires visual experience before eye opening

To gain insight into the role that visual experience plays in the normal function of both rod and cone circuits, we recorded rod-dominant and cone-dominant ERGs from WT mice raised in normal, cyclic lighting conditions (12-h light/12-h dark) and from mice deprived of light (24-h dark) up to P14 and into adulthood (≥P30). A summary of the properties of rod-dominated, cone-dominated, and their downstream ON bipolar cell responses across all conditions are listed in Table 1. Here, we generated intensity-response relations from both a- and b-wave amplitudes, quantified synaptic transfer functions, measured amplification constants from the a-wave, and measured the time photoreceptors spent in saturation to determine if dark-rearing imposed any functional consequences on retinal sensitivity, phototransduction activation, and phototransduction deactivation, respectively.

At P14, rod responses from normal-reared and dark-reared retinas exhibited similar characteristics in both their a- and b-wave properties. Overall, dark rearing did not significantly alter the rod-driven sensitivity of a- or b-waves nor did dark rearing alter amplification rates taken from rod-driven a-waves at P14 or in adulthood (Figs. 5 and 6). However, it cannot be ignored that these same rod-dominated a-waves exhibited a significantly longer time under saturation in P14 dark-reared retinas when compared with normal-reared retinas (n = 12, P < 0.001; Fig. 5 E). To gain deeper insight into how dark rearing may affect the rod signaling pathway, we next quantified b-wave:a-wave ratios and the synaptic transfer function, both of which provide a measure of information transfer from rods to their second-order rod bipolar cells. We found that at dim light intensities, dark-reared retinas exhibited a reduced b-wave:a-wave ratio at P14 compared to normal-reared retinas (Fig. 5 C). However, dark rearing did not significantly alter the synaptic transfer function (k_{nr} = 18.8 μV; k_{dr} = 17.4 μV; Fig. 5 F). Furthermore, in adult retinas, dark rearing did not alter the rod-driven b-wave:a-wave ratio (Fig. 6 C) or the synaptic transfer function (k_{nr} = 5.9 μV; k_{dr} = 4.3 μV; Fig. 6 F).

Next, to determine if dark-rearing alters photopic signaling, we conducted similar studies as those discussed above, but this time with brighter flashes of light superimposed over a rod-saturating background for isolation of cone responses. In contrast to the negligible effects on rod signaling, dark rearing significantly altered cone signaling, most notably at transmission from cones to their bipolar cells. At P14, dark-rearing had already dampened cone-evoked b-waves in response to the brightest flashes (Fig. 7, A and B). Similarly, sensitivity also fell significantly, but primarily at the brightest intensities (n = 12 and 11, P = 1.1452 × 10^{-9}; Fig. 7 B). However, dark rearing did not alter cone-mediated a-wave amplitudes, sensitivities (Fig. 7, D and E), or activation rates (Fig. 7 D, insets). To further probe the functional reduction to signal transmission from cones to cone bipolar cells, we next quantified b-wave:a-wave ratios and the synaptic transfer function. We found that at P14, dark-rearing did reduce the b-wave:a-wave ratio and the sensitivity of the cone bipolar cells (k_{nr} = 26.4 μV; k_{dr} = 18.8 μV; Fig. 7, C and F).

Interestingly, the diminishing effect on b-wave amplitudes in dark-reared retinas became increasingly prominent into adulthood. At maturity, cone-dominated responses exhibited a significantly reduced b-wave across all but the dimmest intensity in dark-reared retinas compared with their normal-reared counterparts (n = 14 and 7, P = 2.6421 × 10^{-10}; Fig. 8, A and B). However, this reduction of the cone-mediated b-wave in dark-reared retinas was not accompanied by any alterations to phototransduction amplification (Fig. 8 D, insets) or a-wave sensitivity (Fig. 8 E). However, dark-reared retinas did in fact exhibit inconsistent reductions in their a-wave amplitudes (Fig. 8 E, open circles). Most notably, in adult retinas, dark rearing significantly reduced the cone bipolar cell sensitivity to these photoreceptor inputs (k_{nr} = 11.4 μV; k_{dr} = 33.1 μV; Fig. 8 F).

The underlying cause of this inconsistent reduction to the a-wave is unclear, but it is evident that dark rearing does affect either postsynaptic component(s) or a presynaptic component(s) outside of the activation of the phototransduction cascade, resulting in altered transmission and a reduced b-wave that manifests by P14 and becomes more evident into maturity.

Sensory deprivation alters specific functional properties of photoreceptors

To further probe the effects of dark-rearing on the nuances of photoreceptor function, we next focus our analysis on the dim flash-evoked a-waves from both rods and cones (Fig. 9 A). From these responses, we quantified several aspects of response kinetics including time-to-peak (t_{peak}), recovery time constant (τ_{rec}), and integration time (t_{int}; Fig. 9, B–D). A summary of these results is also listed in Table 1.

As expected, in normal-reared adult retinas, rod-evoked a-waves exhibited slower dim flash activation kinetics than cones ($t_{peak,\ rods}$: 237 ± 16 ms; $t_{peak,\ cones}$: 64 ± 2 ms; Fig. 9, A and B). Similarly, rods both recovered slower and integrated their responses over a much longer duration than cones (351 ± 30 ms and 314 ± 29 vs. 94 ± 14 ms; Fig. 9 D). There were only two notable changes that dark rearing imposed directly on the functional properties of photoreceptor responses. First, as mentioned earlier, there was a substantial increase in the dominant time constant of rod-evoked responses from dark-reared retinas at eye opening (Fig. 5 D), and this sluggish recovery did not persist into adulthood and this effect was not reflected in any other metric of dim-flash rod recovery in dark-reared retinas (Fig. 9, A, C, and D). On the other hand, cone-driven a-waves did exhibit a slower t_{peak} at maturity in dark-reared retinas (n = 10 and 16, P = 0.0025, 64 ± 2 ms and 90 ± 8 ms; Fig. 9, A and B). The sluggish nature of the cone a-waves in dark-reared retinas may reflect molecular alterations to the photoreceptors themselves, which is likely due to changes in the phototransduction shutoff mechanism or, alternatively, to a component downstream of phototransduction considering that the amplification rates were not significantly altered.

Discussion

This study presents the first comprehensive characterization of light-evoked responses from first-order photoreceptors and

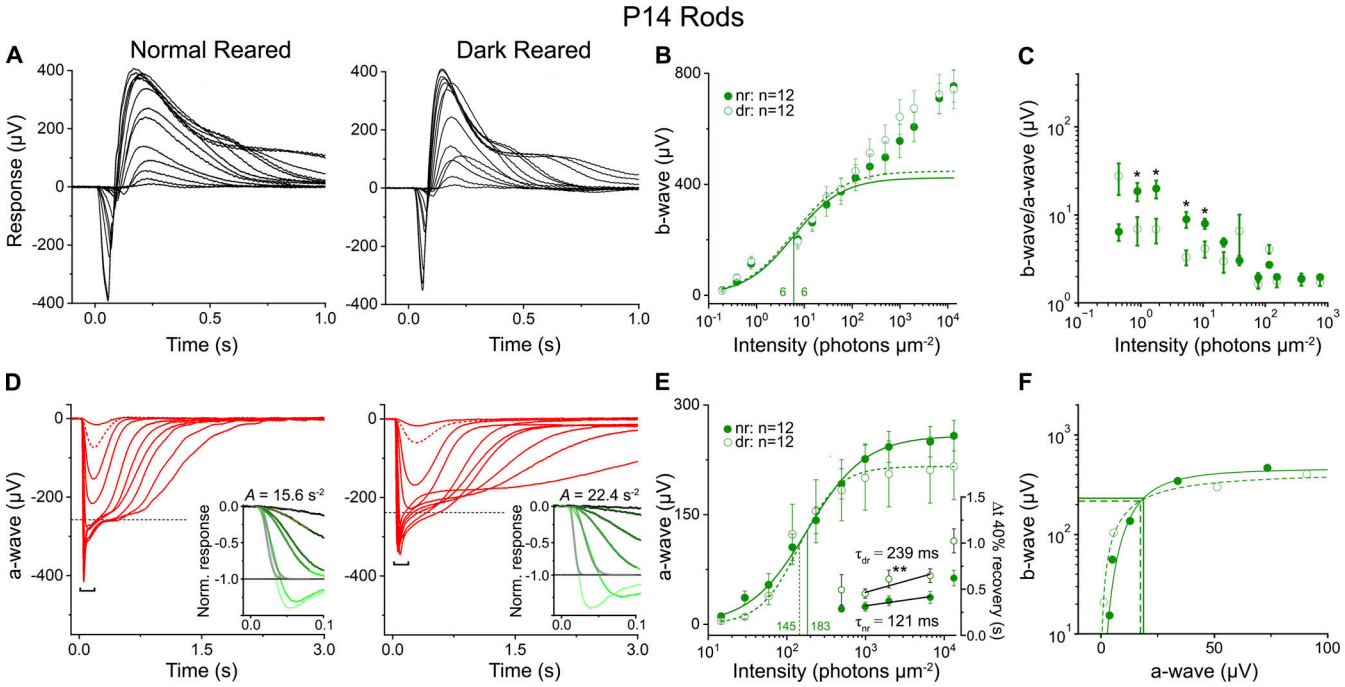

Figure 5. **Dark rearing slows rod response recovery at eye opening.** Rod-dominated ERGs from normal-reared and dark-reared retinas at P14. **(A and B)** Dark rearing does not alter the rod-dominated b-wave amplitude or sensitivity. Initial stimuli provided short (1–8 ms) flashes of 520 nm light (delivering 0.19–13,280 photons μm^{-2}). **(B)** Population averaged b-wave amplitudes from normal-reared (nr, closed circles; *n* = 12 retinas) and dark-reared (dr, open circles; *n* = 12 retinas) mice plotted against flash intensities. **(C)** Dark-rearing reduces the b-wave:a-wave ratio at dim light intensities. Ratios were averaged from normal-reared (nr, closed circles; *n* = 12 retinas) and dark-reared animals (dr, open circles; *n* = 12 retinas) and plotted as a function of light intensity. **(D)** Dark-rearing slows the recovery phase of the rod-dominated a-wave but does not alter the phototransduction amplification rates. Blockers were perfused, and the 10 strongest flashes from A elicited a-waves (red traces). Insets: Activation phase of the a-waves taken from the region indicated by the black bracket on an expanded time scale (*t* = 0–100 ms). These a-waves were normalized to R_{max} after the nose component and fit (superimposed gray traces) with the activation model of phototransduction (Eq. 4) to obtain amplification constants (*A*; s^{-2}). The dashed horizontal indicates response saturation (R_{max}) after the nose component. **(E)** Dark-rearing slows the recovery phase of the rod-dominated a-wave but does not alter sensitivity. Population averaged a-wave amplitudes, along with their recovery times from saturation, in normal-reared (closed symbols; *n* = 12 retinas) and dark-reared (open symbols; *n* = 12 retinas) retinas plotted against flash intensities. Intensity–response relationships were best-fit with Eq. 2 and appear as follows: nr (solid green), dr (dashed green). Vertical lines = half-saturating intensities ($I_{1/2}$). Average time constants (τ_D) were then obtained from a Pepperberg analysis and compared linear fit values (black line) giving the following values: (P14: *n* = 12, P = 0.0049, τ_{nr} = 121 ± 38 ms, τ_{dr} = 239 ± 90 ms). **(F)** Dark rearing does not alter the synaptic transfer function. Representative synaptic transfer functions from a single normal-reared and dark-reared retina were fit with Eq. 6 and appear as follows: nr (solid green), dr (dashed green). Vertical lines = half-saturating a-wave values (solid line: k_{nr} = 18.8 μV; dashed line: k_{dr} = 17.4 μV). Error bars represent mean ± SEM. Single and double asterisks indicate P values of <0.05 and <0.01, respectively.

second-order bipolar cells across postnatal development of the mouse retina. With ex vivo ERGs, we demonstrate that cones respond to light at P8, photoreceptor outputs drive bipolar cell responses by P9, and the relative contributions of rods and cones to the ERG, as well as their response properties depend on postnatal age. Furthermore, we provide physiological evidence for the requirement of light exposure in the developing mouse retina and discovered that the normal function of cone-to-bipolar cell transmission requires early postnatal light exposure while rods do not. We then quantify several response properties highlighting any nuanced light-driven dependencies on the development of photoreceptor and ON bipolar cell response kinetics. We found that dark-rearing slows the cone response when compared with normal-reared animals. Overall, our findings lay out the development of photoresponsivity of the mouse retina and subsequently unveil activity-dependent requirements of the outer retina that have not been described previously.

The use of ex vivo ERGs and isolation of cone-evoked responses

Although similar measurements can be made with various recording techniques, there are three primary reasons we chose ex vivo ERGs for this study. First, photocurrent recordings from photoreceptor outer segments (OS) with the suction electrode technique are impractical as the OS is minute before P10 (LaVail, 1973; Carter-Dawson and LaVail, 1979a; Fei, 2003). Second, whole-cell patch-clamp recordings are ideal but technically demanding, since cones represent only ∼3% of the photoreceptors in the mouse retina (Applebury et al., 2000) and are "lost" amongst the rods (Carter-Dawson and LaVail, 1979a; Carter-Dawson and LaVail, 1979b). However, it is possible to identify cones with a fluorescent reporter (Nikonov et al., 2005; Nikonov et al., 2006), but the light required to do so would strongly desensitize the immature photoreceptors. Moreover, it was only recently demonstrated how to perform such recordings from unlabeled cones (Ingram et al., 2019). Lastly, in vivo ERGs

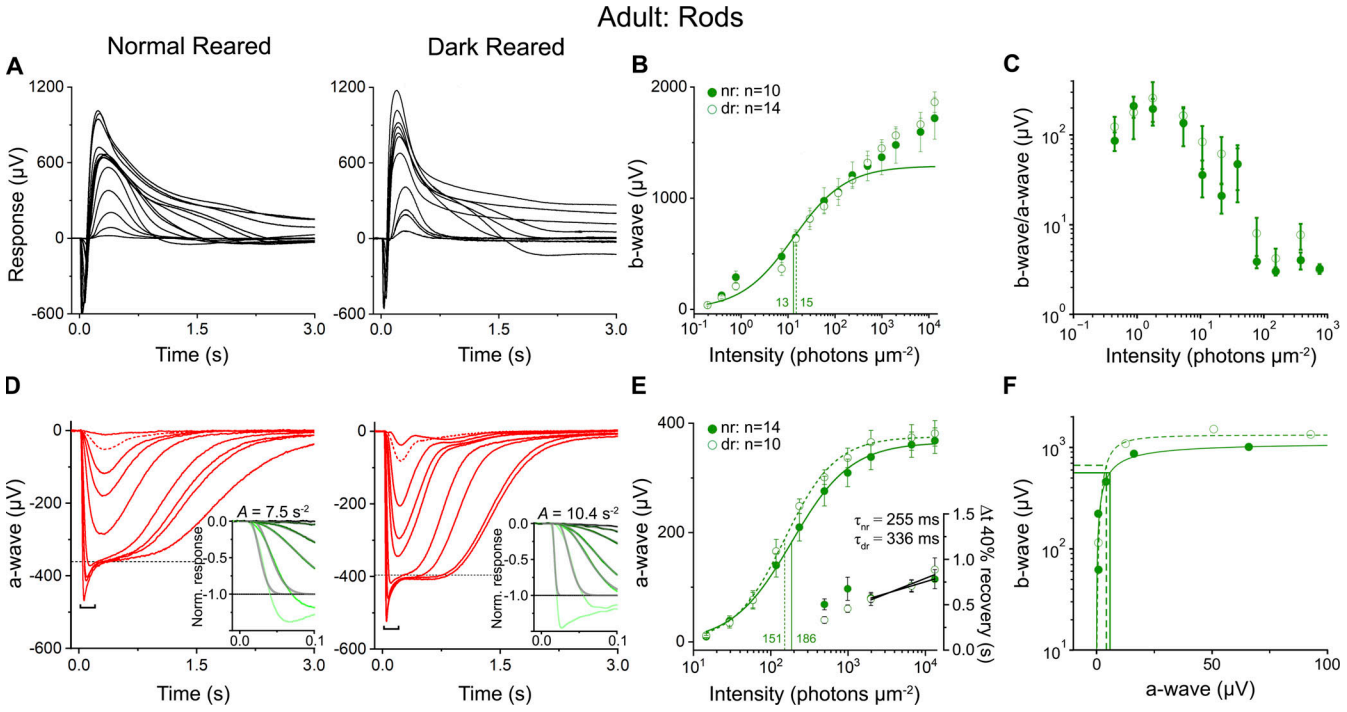

Figure 6. **Dark rearing into maturity does not alter rod-driven responses.** Rod-dominated ERGs from normal-reared and dark-reared adult retinas. **(A and B)** Dark rearing into adulthood does not alter rod-driven b-wave properties. Identical stimulus series from Fig. 5 A elicited b-waves. **(B)** Population averaged b-wave amplitudes from normal-reared (nr, closed circles; *n* = 10 retinas) and dark-reared (dr, open circles; *n* = 14 retinas) retinas plotted against flash intensities. **(C)** Dark rearing into maturity does not alter the b-wave:a-wave ratio. Response ratios represent averages from normal-reared (nr, closed circles; *n* = 11 retinas) and dark-reared (dr, open circles; *n* = 11 retinas) animals plotted as a function of light intensity. **(D)** Dark rearing into adulthood does not alter rod-driven a-wave properties. Blockers were perfused, and the 10 strongest flashes from A elicited a-waves. Insets utilize the same method as Fig. 5 C to obtain the amplification constant (*A*; s^{-2}). **(E)** Dark-rearing does not alter rod-driven a-wave sensitivity and response recovery returns to normal. Population averaged a-wave amplitudes from normal-reared (closed circles; *n* = 12) and dark-reared (open circles; *n* = 12) retinas plotted against flash intensity. Intensity–response relationships were best-fit with Eq. 2 and appear as follows: nr (solid green), dr (dashed green). Vertical lines = half-saturating intensities ($I_{1/2}$). Lower right: Average time constants (τ_D) from a Pepperberg analysis and resultant linear fit values (black line) are reported as follows: adult: *n* = 14 and 10, ns, τ_{nr} = 255 ± 4 ms, τ_{dr} = 336 ± 84 ms. **(F)** Dark rearing does not alter the synaptic transfer function. Representative synaptic transfer functions from a single normal-reared and dark-reared retina were fit with Eq. 6 and appear as follows: nr (solid green), dr (dashed green). Vertical lines = half-saturating a-wave values (solid line: k_{nr} = 5.9 μV; dashed line: k_{dr} = 4.3 μV). Plot values represent mean ± SEM.

generally exhibit both a lower sensitivity and signal-to-noise ratio (SNR), making ex vivo ERGs most suited for detecting smaller, near-threshold responses from developing retinas (Kolesnikov and Kefalov, 2012; Sakurai et al., 2016; Bonezzi et al., 2018). Therefore, ERGs provide several benefits over other recording techniques when considering the objectives of the current study. However, one major limitation remains: it is difficult to extract mechanistic conclusions from extracellular changes in voltage from populations of retinal neurons compared with recordings of intracellular currents from single cells.

The nature of the ERG provides that both rod and cone signals may contribute to the waveform under certain conditions i.e., at mesopic–photopic stimulus intensities. It must be stated that due to the uncertainty of rod sensitivity at early developmental time points, we were unable to use a rod-saturating background on P8 and P9 retinas as illustrated in an adult retina (Fig. 1). We conducted several experiments testing the use of such a background light at these ages (data not shown) but were unable to determine the optimal background that would both suppress rod contributions to the waveform while simultaneously permitting viable cone responses. On the other hand, in P14 and adult retinas, it became much easier to determine the optimal rod-saturating background to use. The rod-mediated nose component and the rod "arm" of the intensity response curve are strong indicators of rod saturation. These were more robust further into development and permitted a good estimation of rod response suppression, although, it must be noted that rods can escape such saturation in certain cases (Tikidji-Hamburyan et al., 2017). However, considering the brightness of the background steps used here, it remains unlikely that rods were able to escape saturation and likely contributed negligibly to the ERG. To further support this notion, the cone-evoked response threshold emerged under mesopic intensities and continued far into the photopic range, with initial responses evoked at 563 photons per μm^2 and with saturation occurring at 233,733 photons per μm^2 ($I_{1/2}$ = 11,495 ± 130 photons per μm^2), which is consistent with cone function in brightly lit conditions.

Physiological properties of light-evoked activity before eye opening

The nature of the ERG from mice before eye opening was generally dissimilar in waveform and kinetics to that of retinas from

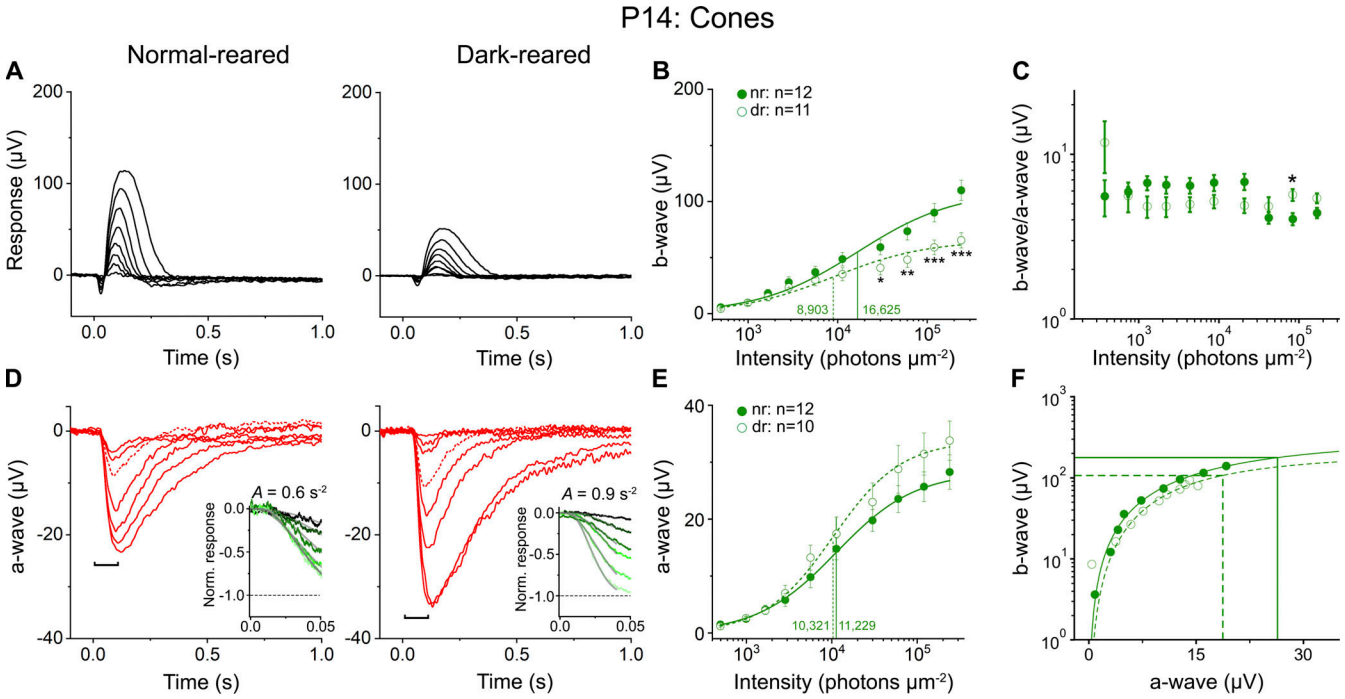

Figure 7. **Dark rearing reduces cone transmission at eye opening.** Cone-dominated ERGs from normal-reared and dark-reared P14 retinas. **(A and B)** Dark-rearing reduces the cone-driven b-wave at the brightest light intensities. Stimulus families provided short (1–8 ms) photopic flashes of 520 nm light (delivering 495–239,594 photons μm^{-2}). Responses were isolated using the protocol in Fig. 1. **(B)** Population averaged b-wave amplitudes plotted as a function of flash intensities from normal-reared (nr, closed circles; n = 12 retinas) and dark-reared (dr, open circles; n = 13 retinas) mice. **(C)** Dark-rearing does not significantly alter the b-wave:a-wave ratio. Response ratios represent averages from normal-reared (nr, closed circles; n = 10 retinas) and dark-reared (dr, open circles; n = 10 retinas) animals plotted as a function of light intensity. **(D)** Dark-rearing does not alter cone-driven a-wave properties. Blockers were perfused and the same stimulus families from A elicited a-waves (red traces). Insets: Rising phase of the a-wave (black bracket) on an expanded time scale, normalized to $R_{max,}$ and fit (superimposed gray traces) with Eq. 4 to obtain the amplification constant (A; s^{-2}). Dashed horizontal = response saturation (R_{max}). **(E)** Population averaged a-wave amplitudes plotted as a function of flash intensity from normal-reared (nr, closed circles; n = 12 retinas) and dark-reared (dr, open circles; n = 10 retinas) mice. Intensity–response relationships were best-fit with Eq. 2 and fit lines appear as follows: normal reared (solid green) and dark reared (dashed green). Vertical lines = half-saturating intensities ($I_{1/2}$). **(F)** Dark rearing does not alter the synaptic transfer function. Representative synaptic transfer functions from a single normal-reared (closed circles) and dark-reared (open circles) retina fit with Eq. 6 and appear as follows: nr (solid green), dr (dashed green). Vertical lines = half-saturating a-wave values (solid lines: k_{nr} = 26.4 μV; dashed lines: k_{dr} = 18.8 μV). Error bars represent mean ± SEM. Single, double, and triple asterisks indicate P values of <0.05, <0.01, and <0.001, respectively.

mature mice (Fig. 2). Below, we discuss a few primary factors which may contribute to the uniqueness of these photoresponses obtained from photoreceptors and bipolar cells and may also complicate the interpretation of these results.

First, the photoreceptor OS emerges at P8 and elongates linearly with age reaching adult length around P30. For example, a rod OS at P8 is less than a micron in length compared with that at P30 (~20 μm; Obata and Usukura, 1992). The OS membrane surface area, and therefore, the collecting area (a_c) of an immature rod or cone is dramatically reduced compared with those of mature photoreceptors. However, this applies more to rods, as the cone OS is shorter and therefore reaches adult lengths much earlier in development. As a result, an immature rod has a proportionally smaller dark current, and it should be expected that rods will generate an equivalently smaller a-wave. However, it should be stated that it remains uncertain what the exact a_c of these developing photoreceptors was; therefore, we limit any mechanistic conclusions from data collected from P8–P10 retinas. Because the retina is detached from the RPE for ex vivo ERGs, RPE-mediated pigment regeneration is absent when compared with in vivo or eyecup preparations (Pepperberg et al., 1978; Vinberg et al., 2014). Müller cells can aid in some pigment regeneration (Wang and Kefalov, 2011; Frederiksen et al, 2021). However, it is unknown to what extent developing retinas are capable of pigment regeneration arising from the RPE versus from Müller cells. Due to a relatively immature visual cycle before P14, rods at this age contain high amounts of free opsin, which lacks the light-sensitive chromophore, resulting in seemingly desensitized rods compared to cones (Luo and Yau, 2005).

Keeping these factors in mind, several characteristics of these responses indicate that both rod and cone-driven activities together generate the ERG waveform before eye opening. First, the mesopic–photopic threshold for light responses as well as the cone-like t_{peak} values observed at P8 suggests cone-driven activity while the sluggish response recovery reflects a rod-like response. In the case that it is a "purely" cone-evoked response, the sluggish recovery indicates that a component of the phototransduction machinery may be insufficiently expressed. Further support of this notion arises from Fig. 2 A, where we demonstrate that P8 *Gnat1*$^{-/-}$ retinas exhibit similarly sized responses compared with P8 WT retinas. Certain genes coding for

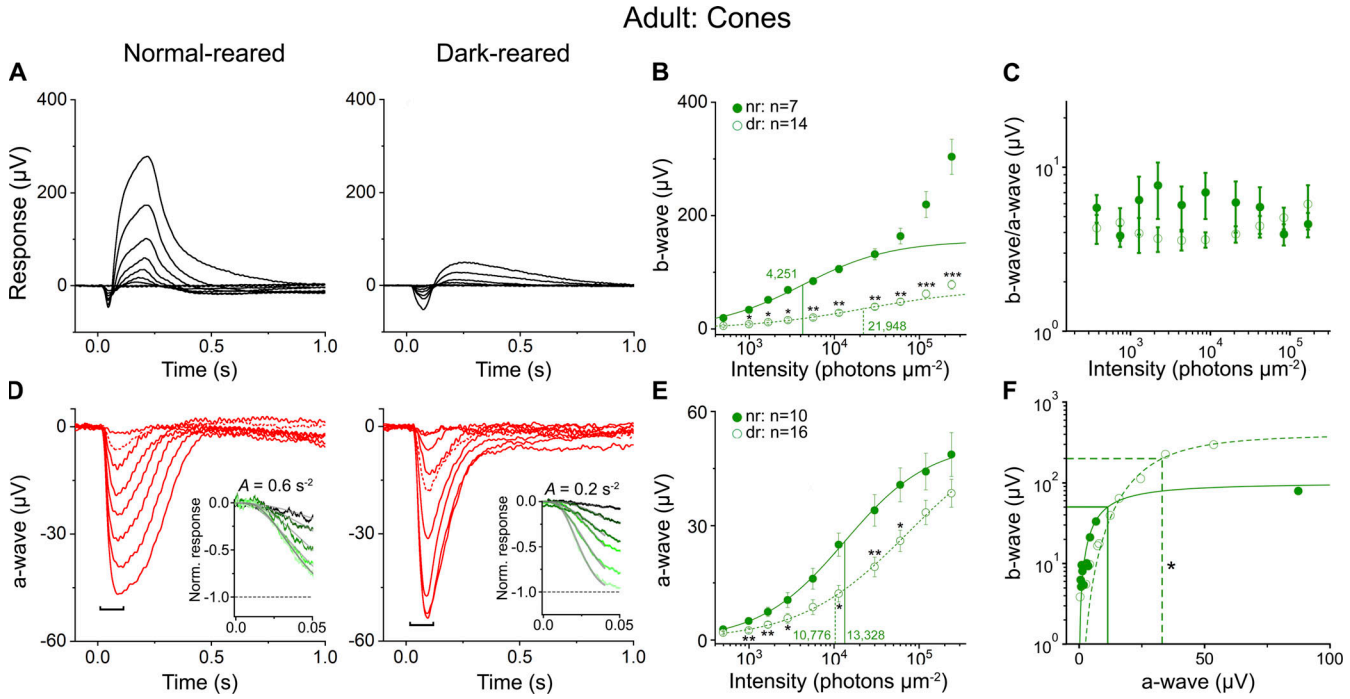

Figure 8. **Sensory deprivation into maturity further diminishes the cone-mediated b-wave.** Cone-dominated ERGs from normal-reared and dark-reared adult retinas under identical stimulus conditions from Fig. 7. **(A and B)** Dark rearing into adulthood nearly eliminates transmission from cones to their bipolar cells across all light intensities. **(B)** Population-averaged cone-driven b-wave amplitudes plotted against flash intensity from normal-reared (nr, closed circles; n = 7) and dark-reared (dr, open circles; n = 14) retinas. **(C)** Dark rearing does not alter the b-wave:a-wave ratio. Response ratios represent averages from normal-reared (nr, closed circles; n = 10 retinas) and dark-reared (dr, open circles; n = 10 retinas) animals plotted as a function of light intensity. **(D)** Dark rearing alters cone-driven a-waves. Blockers were perfused and the same stimulus families used in A elicited a-waves (red traces). Insets utilize the same method as Fig. 7 C to obtain amplification constants (A; s^{-2}). The dashed horizontal indicates response saturation (R_{max}). **(E)** Cone-driven a-wave amplitudes are reduced at most light intensities while their sensitivity remains normal. Intensity–response relationships were best-fit with Eq. 2 and appear as follows: nr (solid green), dr (dashed green). Half-saturating intensities ($I_{1/2}$) = vertical lines. **(F)** Dark rearing reduces the sensitivity of synaptic transmission. Representative synaptic transfer functions from a single normal-reared (closed circles) and dark-reared (open circles) retina. The synaptic transfer function was fit with Eq. 6 and appear as follows: nr (solid green), dr (dashed green). Vertical lines = half-saturating a-wave values (solid lines: k_{nr} = 11.4 μV; dashed lines: k_{dr} = 33.1 μV). Average half-saturating a-waves from all retinas (k_{nr} = 15.7 μV, k_{dr} = 33.3 μV; P = 0.02). Error bars represent mean ± SEM. Single, double, and triple asterisks indicate P values of <0.05, <0.01, and <0.001, respectively.

proteins involved in phototransduction are expressed at low levels during this point in development (Blackshaw et al., 2001; Blackshaw et al., 2004; Aavani et al., 2017), making it possible that the sluggish response recovery results from the insufficient expression of a component intricately linked to response shutoff such as guanylate cyclase-activating proteins (GCAPs; Howes et al., 2002). The relative brightness of the flashes used at P8 (see Materials and methods) may have also contributed to this slow recovery considering that brighter light will inherently bleach more pigment molecules, resulting in a slower recovery time. All things considered, it is much more likely that cones drive the P10 responses evoked under background light as these responses exhibited faster activation and deactivation kinetics compared with recordings from single rods at P12 (Table 1; $t_{peak;\ cones}$ = 43 ± 4.5 ms and $t_{int;\ cones}$ = 146 ± 29 ms vs. $t_{peak;\ rods}$ ~200 ms and $t_{int;\ rods}$ ~290 ms; Luo and Yau, 2005; Fig. 3 C). On the other hand, in the absence of background light, P10 response kinetics were much slower and compare more closely to those previously published results (Table 1; $t_{peak;\ rods/cones}$ = 147 ± 17 ms and $t_{int;\ rods/cones}$ = 234 ± 20 ms). Additionally, the sensitivity of our P10 responses under background light was over two orders of magnitude lower than those in the presence of background light (12,711 ± 1,835 compared to 27 ± 12 photons μm^{-2}) and these responses did not display a prominent nose component as the rod-dominated traces did (Fig. 2 A). To further support this and validate the effectiveness of our use of background light, data collected from *Gnat1*$^{-/-}$ mice at P10 exhibited similar response amplitudes to WT (Table 1; P10 *Gnat1*$^{-/-}$ $R_{max;\ cones}$ 13.9 ± 4.7 $R_{dim;\ cones}$ 4.1 ± 1.5). However, their time to peak was much slower (Table 1; P10 $t_{peak;\ cones}$ = 332.3 ± 45.7 ms and $t_{int;\ cones}$ = 302.1 ± 21.5 ms). Previous findings agree with this, where the time to peak and *Gnat1*$^{-/-}$ mouse cones are slower than cones in the WT animal (Calvert et al., 2000; Ingram et al., 2019). This potentially is explained by crosstalk between rod and cone photoreceptors via gap junctions. We speculate that at the level of the ERG, this slowdown manifests in a much slower time to peak than would be expected for cones. A potential avenue of further study is to utilize a *Gnat1*$^{-/-}$ and connexion-36 (*Cx36*$^{-/-}$; Asteriti et al., 2017)

Furthermore, we suspect that the minute nose component observed at P9, which becomes more robust by P10 (Figs. 2 and 3), reflects the emergence of rod-driven activity. There is no change in recovery as the retina matures from P9 to the adult retina (Fig. 4 C). This is not surprising as the faster cone

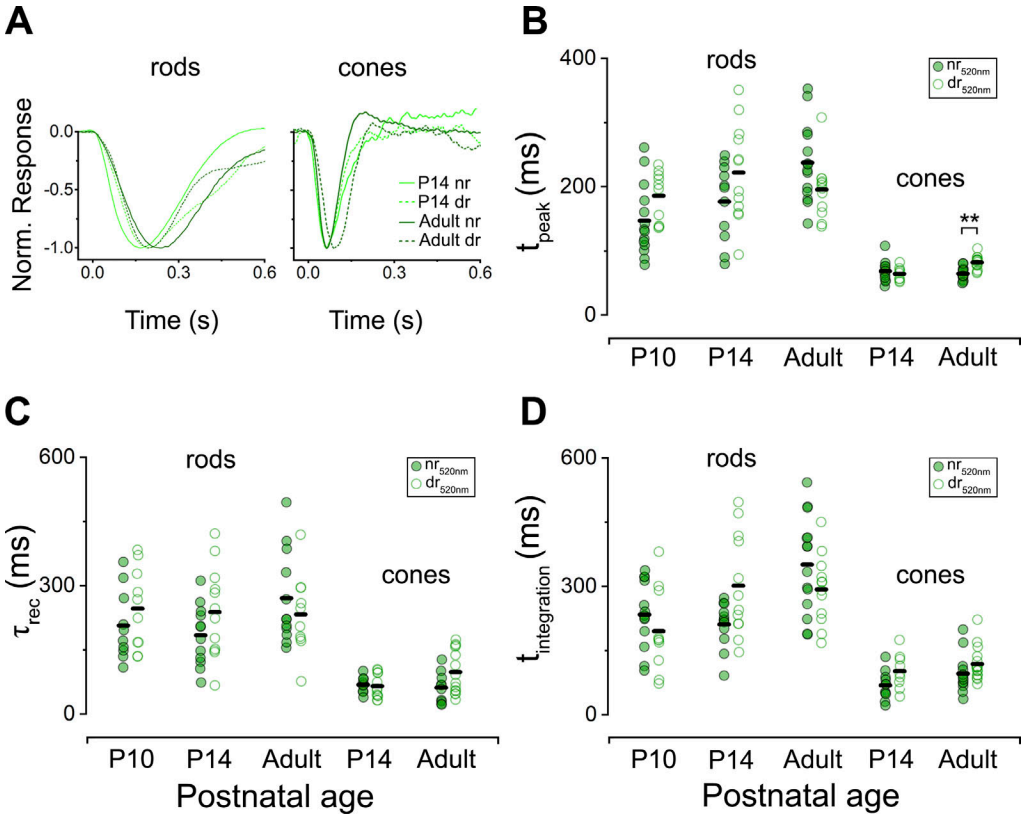

Figure 9. **Light deprivation into adulthood slows cone-driven responses.** Dim flash kinetics of rod and cone responses from normal-reared (nr) and dark-reared (dr) retinas calculated from R_{dim} (see Materials and methods). **(A)** Normalized, representative rod- (left) and cone-driven (right) a-waves in response to dim flashes illustrate waveform kinetics at P14 and maturity. **(B–D)** Individual retina response properties to dim flashes (closed = nr, open = dr) plotted across postnatal age. **(B)** Exclusively, mature cone responses in dark-reared retinas exhibited a significant increase in t_{peak} (adult, cones: n = 10 and 16, P = 0.0025, 64 ± 2 ms and 90 ± 8 ms). **(C and D)** Dark-rearing had little effect on the recovery time constant (τ_{rec}; C) and integration times (t_{int}; D) in both rod- and cone-driven responses. The black bar represents the population mean. Double asterisks indicate a P value of <0.01.

recovery time would be masked behind the rod recovery time, even if the a-wave were cone-dominated. This masking effect of the rod recovery results in an increase in the integration time which at first may seem counter-intuitive (Fig. 4 D). The amplitude difference between the adult WT and adult *Gnat*$^{-/-}$ (adult WT, n = 14, 368 ± 23 µV; adult *Gnat*$^{-/-}$, n = 7, 37.2 ± 4.5 µV) indicates that the cone response only makes up about 10% of the adult a-wave. Together, these data suggest that cones make up an appreciable percentage of the total emerging a-wave response (P8–P10), while in the mature retina, the a-wave is dominated by rod responses.

Aside from photoreceptor-driven activity, the BTR also shapes the scotopic waveform starting at P9. For mature tissue, in which bipolar cells pool activity from 20 to 100 photoreceptors (Okawa and Sampath, 2007), the resulting b-wave typically dwarfs the a-wave. However, this immature b-wave observed at P9 is comparatively much smaller, likely due to sparse connectivity with second-order cells. Since ON bipolar cells depolarize in the presence of light, it is likely that the earliest bipolar cells to complete synaptogenesis (Blanks et al., 1974; Sharma et al., 2003; Regus-Leidig et al., 2009) with their presynaptic partners, generated this positive-going pull on the waveform. As such, at P9, responses to scotopic intensities exhibit a positive going amplitude that is approximately equal and opposite in amplitude to the photoreceptor-driven a-wave resulting in an atypical b-wave which does not cross baseline as it does at P10 (Fig. 3, A and C). Local ERG recordings have demonstrated similarly shaped waveforms where one component of the ERG out-drives the other (Turunen and Koskelainen, 2017). Interestingly, the rising phase of the negative-going a-wave in the absence of synaptic blockers compared to the a-wave in the presence of blockers (Fig. 3 A, scotopic dark traces vs. scotopic red traces) does not superimpose with one another as they do at P10. The reason this pulling effect is not as evident at P10 (although remains at scotopic intensities), is speculative, but it is possible that as more rods become functional at P10, more rods contribute to the a-wave. As such, this increasing shift toward a rod-dominated ERG exhibits a slower t_{peak} (see Table 1; $P9_{rods/cones}$: 116 ± 24 vs. $P10_{rods/cones}$: 147 ± 17), making it such that the onset of the a-wave and b-waves don't coincide temporally as they do even a day prior. Therefore, the immature b-wave at P10 does not have as dramatic of an effect on the waveform at lower light intensities on the a-wave as it did at P9.

The role of visual experience in the maturation of rod and cone signaling

We found that rod- and cone-dominated responses in mature, normal-reared retinas paralleled those of previous studies

conducted under similar recording conditions (Heynen et al., 1985; Ekesten et al., 2001; Heikkinen et al., 2008; Heikkinen et al., 2012; Vinberg et al., 2014; Vinberg and Kefalov, 2015; Sakurai et al., 2016; Turunen and Koskelainen, 2017).

In contrast, dark rearing altered this normal responsivity of rod and cone signaling in both obvious and subtle ways. As mentioned, rod signaling was minimally affected by dark rearing overall; however, the time that rods spent under saturation was significantly longer than those of normal-reared animals (Fig. 5 E). This increase in time under saturation could reflect a time-dependent window for light influence on photoreceptor development or it could, more likely, reflect the increased dark-adapted state of the dark-reared animals. Interestingly, we did not find that the rod-dominated b-waves were reduced in mature animals (≥P30) as they were in a previous study from dark-reared animals at P30 (Vistamehr and Tian, 2004). It is likely that because we did not confine these measurements to animals that were precisely 30 d old, and we instead averaged responses collected from animals aged anywhere from P30–P60 for our mature subjects, we may have missed the time point for this previously observed reduction to the b-wave.

More interestingly, the cone pathway suffered the utmost detriment to second-order signaling, as dark rearing resulted in dampened b-waves at P14 and diminished these b-waves to a greater degree at maturity (Figs. 7 and 8). In agreement with this data, dark-reared adult retinas exhibited a b-wave which was significantly desensitized to cone inputs (Fig. 8 F). Together, these findings support a similar dependency on visual experience for the normal development of mammalian cone signaling as previous reports (Baxter and Rissen, 1961; He et al, 2011). More specifically, these data support the hypothesis that properly timed photopic light-evoked activity, i.e., visual experience before eye opening, is required for normal synaptogenesis between cones and certain postsynaptic partners (Dunn and Wong, 2012; Dunn et al., 2013). Moreover, the cone-specific reduction to second-order signaling raises an interesting question: Why does the developing retina require light-evoked input for the refinement of certain intraretinal circuits but not for others which hardwire earlier in development, seemingly unbothered by light deprivation? One possibility is that constant neurotransmission in the dark yields the desensitization of postsynaptic mGluR6 receptors, resulting in faulty wiring. Alternatively, it may be that the developing retina is sensitive to changes in the temporal properties of light-evoked activity of cones and the associated glutamate release rates within the OPL. Therefore, this preferential effect between developing rod and cone pathways could result from differing requirements of glutamatergic signaling patterns, like the phenomena demonstrated in previous reports (Myhr et al., 2001; Kerschensteiner et al., 2009).

Furthermore, upstream alterations to photoreceptor components that transform the photocurrent signal at the inner segment, and additionally near the terminal, could tune the continuous release of glutamate from photoreceptors in darkness (Fain and Sampath, 2021). However, few studies have demonstrated a developmental requirement of light input for normal photoreceptor function, although others have demonstrated such experience-based requirements in first-order olfactory neurons (He et al., 2012). Our data loosely support such a requirement, as both rod- and cone-driven a-waves in dark-reared retinas exhibited some form of physiological detriment (Fig. 5, D and E; Fig. 8 E; and Fig. 9 B).

However, the sluggish rod recovery seen (Fig. 5, D and E) disappeared with maturation, indicating that there may be a developmental window for such a light dependency. On the other hand, cone-evoked dim flash responses in dark-reared animals displayed slower t_{peak} even into adulthood (Fig. 9, A and B). Because cones are inherently less sensitive to incoming photons, they operate primarily in bright light; therefore, the proper development of their downstream circuitries may similarly require activities driven by higher photic input. Although unclear, the sluggish cone response may contribute to synaptic plasticity which depends on cone output rates, as normal circuit formation has been linked to requirements of specific neurotransmitter release rates in the inner retina (Kerschensteiner et al., 2009; Soto et al., 2012). Therefore, a functional consequence of altered photoreceptor output rates during this developmental window may underlie circuit alterations, thus leading to the reduced ON bipolar cell gain seen here. Unfortunately, it is difficult to make such conclusions from ERGs and this may be better answered with whole-cell patch-clamp recordings.

Overall, these findings describe the developmental progression of first- and second-order cellular responsivities in mouse retina and supplement the existing knowledge base that describes the requirements of visual experience in the developing mammalian visual system. Our data contradict the notion that light-evoked activity of the outer retina is absent before P10 (Tian and Copenhagen, 2003; Luo and Yau, 2005) and provide the first direct electrophysiological characterization of such activity along with the subsequent developmental progression of these responses. Therefore, it should be considered that light shining through the closed eyelid of the postnatal mouse can elicit near-threshold responses which drive specific rod/cone output patterns that may play an integral role in transitioning from cholinergic to glutamatergic retinal waves (Wong, 1999; Zhou and Zhao, 2000), intraretinal circuit refinement, and ultimately, higher-order visual system development.

Data availability

The data underlying figures and tables in this manuscript are openly available in G-Node GIN at https://gin.g-node.org/Mattar13/JGP_2023_BonezziTarchick.git.

Acknowledgments

Christopher J. Lingle served as editor.

We thank Jessica Onyak for her daily assistance in the lab and Katelyn Sondereker for proofreading the manuscript. We also thank Ricardo Vargas from Gamma Scientific for helping with light calibrations, as well as Soile Nymark and Norianne Ingram for helpful discussion along the way. We also thank Johnny Tarchick for input on statistics.

This work was supported by National Institutes of Health grant R15EY026255-01.

Author contributions: Ex-vivo ERGs were performed at the University of Akron by P.J. Bonezzi and M.J. Tarchick. J.M. Renna and P.J. Bonezzi conceived the study. P.J. Bonezzi generated the first draft of the manuscript, and it was further revised and edited by J.M. Renna and M.J. Tarchick. All authors contributed meaningfully to the revision and intellectual content, approved the final manuscript, and agreed to be accountable for all aspects of the work.

Disclosures: The authors declare no competing interests exist.

Submitted: 11 September 2022
Revised: 24 February 2023
Revised: 5 April 2023
Revised: 3 May 2023
Revised: 25 May 2023
Accepted: 8 June 2023

References

Aavani, T., N. Tachibana, V. Wallace, J. Biernaskie, and C. Schuurmans. 2017. Temporal profiling of photoreceptor lineage gene expression during murine retinal development. *Gene Expr. Patterns*. 23-24:32–44. https://doi.org/10.1016/j.gep.2017.03.001

Applebury, M.L., M.P. Antoch, L.C. Baxter, L.L. Chun, J.D. Falk, F. Farhangfar, K. Kage, M.G. Krzystolik, L.A. Lyass, and J.T. Robbins. 2000. The murine cone photoreceptor: A single cone type expresses both S and M opsins with retinal spatial patterning. *Neuron*. 27:513–523. https://doi.org/10.1016/S0896-6273(00)00062-3

Asteriti, S., C. Gargini, and L. Cangiano. 2014. Mouse rods signal through gap junctions with cones. *Elife*. 3:e01386. https://doi.org/10.7554/eLife.01386

Asteriti, S., C. Gargini, and L. Cangiano. 2017. Connexin 36 expression is required for electrical coupling between mouse rods and cones. *Vis. Neurosci.* 34:E006. https://doi.org/10.1017/S0952523817000037

Baxter, B.L., and A.H. Rissen. 1961. Electroretinogram of the visually deprived cat. *Science*. 134:1626–1627. https://doi.org/10.1126/science.134.3490.1626

Baylor, D.A., B.J. Nunn, and J.L. Schnapf. 1984. The photocurrent, noise and spectral sensitivity of rods of the monkey Macaca fascicularis. *J. Physiol.* 357:575–607. https://doi.org/10.1113/jphysiol.1984.sp015518

Blackshaw, S., R.E. Fraioli, T. Furukawa, and C.L. Cepko. 2001. Comprehensive analysis of photoreceptor gene expression and the identification of candidate retinal disease genes. *Cell*. 107:579–589. https://doi.org/10.1016/S0092-8674(01)00574-8

Blackshaw, S., S. Harpavat, J. Trimarchi, L. Cai, H. Huang, W.P. Kuo, G. Weber, K. Lee, R.E. Fraioli, S.H. Cho, et al. 2004. Genomic analysis of mouse retinal development. *PLoS Biol.* 2:E247. https://doi.org/10.1371/journal.pbio.0020247

Blanks, J.C., A.M. Adinolfi, and R.N. Lolley. 1974. Synaptogenesis in the photoreceptor terminal of the mouse retina. *J. Comp. Neurol.* 156:81–93. https://doi.org/10.1002/cne.901560107

Bodenstein, L., and R.L. Sidman. 1987. Growth and development of the mouse retinal pigment epithelium. I. Cell and tissue morphometrics and topography of mitotic activity. *Dev. Biol.* 121:192–204. https://doi.org/10.1016/0012-1606(87)90152-7

Bolnick, D.A., A.E. Walter, and A.J. Sillman. 1979. Barium suppresses slow PIII in perfused bullfrog retina. *Vis. Res.* 19:1117–1119. https://doi.org/10.1016/0042-6989(79)90006-3

Bonezzi, P.J., M.E. Stabio, and J.M. Renna. 2018. The development of mid-wavelength photoresponsivity in the mouse retina. *Curr. Eye Res.* 43:666–673. https://doi.org/10.1080/02713683.2018.1433859

Bonezzi, P.J., M.J. Tarchick, and J.M. Renna. 2020. Ex vivo electroretinograms made easy: Performing ERGs using 3D printed components. *J. Physiol.* 598:4821–4842. https://doi.org/10.1113/JP280014

Calvert, P.D., N.V. Krasnoperova, A.L. Lyubarsky, T. Isayama, M. Nicoló, B. Kosaras, G. Wong, K.S. Gannon, R.F. Margolskee, R.L. Sidman, et al. 2000. Phototransduction in transgenic mice after targeted deletion of the rod transducin α-subunit. *Proc. Natl. Acad. Sci. USA*. 97:13913–13918. https://doi.org/10.1073/pnas.250478897

Carter-Dawson, L.D., and M.M. LaVail. 1979a. Rods and cones in the mouse retina. I. Structural analysis using light and electron microscopy. *J. Comp. Neurol.* 188:245–262. https://doi.org/10.1002/cne.901880204

Carter-Dawson, L.D., and M.M. LaVail. 1979b. Rods and cones in the mouse retina. II. Autoradiographic analysis of cell generation using tritiated thymidine. *J. Comp. Neurol.* 188:263–272. https://doi.org/10.1002/cne.901880205

Daum, J.M., Ö. Keles, S.J. Holwerda, H. Kohler, F.M. Rijli, M. Stadler, and B. Roska. 2017. The formation of the light-sensing compartment of cone photoreceptors coincides with a transcriptional switch. *Elife*. 6:e31437. https://doi.org/10.7554/eLife.31437

Dunn, F.A., and R.O. Wong. 2012. Diverse strategies engaged in establishing stereotypic wiring patterns among neurons sharing a common input at the visual system's first synapse. *J. Neurosci.* 32:10306–10317. https://doi.org/10.1523/JNEUROSCI.1581-12.2012

Dunn, F.A., L. Della Santina, E.D. Parker, and R.O. Wong. 2013. Sensory experience shapes the development of the visual system's first synapse. *Neuron*. 80:1159–1166. https://doi.org/10.1016/j.neuron.2013.09.024

Ekesten, B., P. Gouras, and D.J. Salchow. 2001. Ultraviolet and middle wavelength sensitive cone responses in the electroretinogram (ERG) of normal and *Rpe65*−/− mice. *Vis. Res.* 41:2425–2433. https://doi.org/10.1016/S0042-6989(01)00140-7

Fain, G.L., and A.P. Sampath. 2021. Light responses of mammalian cones. *Pflugers Arch.* 473:1555–1568. https://doi.org/10.1007/s00424-021-02551-0

Fei, Y. 2003. Development of the cone photoreceptor mosaic in the mouse retina revealed by fluorescent cones in transgenic mice. *Mol. Vis.* 9:31–42.

Feller, M.B., D.P. Wellis, D. Stellwagen, F.S. Werblin, and C.J. Shatz. 1996. Requirement for cholinergic synaptic transmission in the propagation of spontaneous retinal waves. *Science*. 272:1182–1187. https://doi.org/10.1126/science.272.5265.1182

Fisher, L.J. 1979. Development of synaptic arrays in the inner plexiform layer of neonatal mouse retina. *J. Comp. Neurol.* 187:359–372. https://doi.org/10.1002/cne.901870207

Ford, K.J., and M.B. Feller. 2012. Assembly and disassembly of a retinal cholinergic network. *Vis. Neurosci.* 29:61–71. https://doi.org/10.1017/S0952523811000216

Frederiksen, R., A. Morshedian, S.A. Tripathy, T. Xu, G.H. Travis, G.L. Fain, and A.P. Sampath. 2021. Rod photoreceptors avoid saturation in bright light by the movement of the G protein transducin. *J. Neurosci.* 41:3320–3330. https://doi.org/10.1523/JNEUROSCI.2817-20.2021

Govardovskii, V.I., N. Fyhrquist, T. Reuter, D.G. Kuzmin, and K. Donner. 2000. In search of the visual pigment template. *Vis. Neurosci.* 17:509–528. https://doi.org/10.1017/S0952523800174036

He, Q., P. Wang, and N. Tian. 2011. Light-evoked synaptic activity of retinal ganglion and amacrine cells is regulated in developing mouse retina. *Eur. J. Neurosci.* 33:36–48. https://doi.org/10.1111/j.1460-9568.2010.07484.x

He, J., H. Tian, A.C. Lee, and M. Ma. 2012. Postnatal experience modulates functional properties of mouse olfactory sensory neurons. *Eur. J. Neurosci.* 36:2452–2460. https://doi.org/10.1111/j.1460-9568.2012.08170.x

Heikkinen, H., S. Nymark, and A. Koskelainen. 2008. Mouse cone photoresponses obtained with electroretinogram from the isolated retina. *Vis. Res.* 48:264–272. https://doi.org/10.1016/j.visres.2007.11.005

Heikkinen, H., F. Vinberg, S. Nymark, and A. Koskelainen. 2011. Mesopic background lights enhance dark-adapted cone ERG flash responses in the intact mouse retina: A possible role for gap junctional decoupling. *J. Neurophysiol.* 105:2309–2318. https://doi.org/10.1152/jn.00536.2010

Heikkinen, H., F. Vinberg, M. Pitkänen, B. Kommonen, and A. Koskelainen. 2012. Flash responses of mouse rod photoreceptors in the isolated retina and corneal electroretinogram: Comparison of gain and kinetics. *Invest. Ophthalmol. Vis. Sci.* 53:5653–5664. https://doi.org/10.1167/iovs.12-9678

Heynen, H., L. Wachtmeister, and D. van Norren. 1985. Origin of the oscillatory potentials in the primate retina. *Vis. Res.* 25:1365–1373. https://doi.org/10.1016/0042-6989(85)90214-7

Hornstein, E.P., J. Verweij, P.H. Li, and J.L. Schnapf. 2005. Gap-junctional coupling and absolute sensitivity of photoreceptors in macaque retina. *J. Neurosci.* 25:11201–11209. https://doi.org/10.1523/JNEUROSCI.3416-05.2005

Howes, K.A., M.E. Pennesi, I. Sokal, J. Church-Kopish, B. Schmidt, D. Margolis, J.M. Frederick, F. Rieke, K. Palczewski, S.M. Wu, et al. 2002. GCAP1 rescues rod photoreceptor response in GCAP1/GCAP2 knockout mice. *EMBO J.* 21:1545–1554. https://doi.org/10.1093/emboj/21.7.1545

Hubel, D.H., and D.C. Freeman. 1977. Projection into the visual field of ocular dominance columns in macaque monkey. *Brain Res.* 122:336–343. https://doi.org/10.1016/0006-8993(77)90299-2

Hubel, D.H., T.N. Wiesel, and S. LeVay. 1977. Plasticity of ocular dominance columns in monkey striate cortex. *Philos. Trans. R. Soc. Lond. B Biol. Sci.* 278:377–409. https://doi.org/10.1098/rstb.1977.0050

Huberman, A.D., M. Manu, S.M. Koch, M.W. Susman, A.B. Lutz, E.M. Ullian, S.A. Baccus, and B.A. Barres. 2008. Architecture and activity-mediated refinement of axonal projections from a mosaic of genetically identified retinal ganglion cells. *Neuron.* 59:425–438. https://doi.org/10.1016/j.neuron.2008.07.018

Ingram, N.T., A.P. Sampath, and G.L. Fain. 2016. Why are rods more sensitive than cones? *J. Physiol.* 594:5415–5426. https://doi.org/10.1113/JP272556

Ingram, N.T., A.P. Sampath, and G.L. Fain. 2019. Voltage-clamp recordings of light responses from wild-type and mutant mouse cone photoreceptors. *J. Gen. Physiol.* 151:1287–1299. https://doi.org/10.1085/jgp.201912419

Johnson, J., N. Tian, M.S. Caywood, R.J. Reimer, R.H. Edwards, and D.R. Copenhagen. 2003. Vesicular neurotransmitter transporter expression in developing postnatal rodent retina: GABA and glycine precede glutamate. *J. Neurosci.* 23:518–529. https://doi.org/10.1523/JNEUROSCI.23-02-00518.2003

Kerschensteiner, D., J.L. Morgan, E.D. Parker, R.M. Lewis, and R.O. Wong. 2009. Neurotransmission selectively regulates synapse formation in parallel circuits in vivo. *Nature.* 460:1016–1020. https://doi.org/10.1038/nature08236

Kim, D.S., S.E. Ross, J.M. Trimarchi, J. Aach, M.E. Greenberg, and C.L. Cepko. 2008. Identification of molecular markers of bipolar cells in the murine retina. *J. Comp. Neurol.* 507:1795–1810. https://doi.org/10.1002/cne.21639

Kolesnikov, A.V., and V.J. Kefalov. 2012. Transretinal ERG recordings from mouse retina: Rod and cone photoresponses. *J. Vis. Exp.* 3424. https://doi.org/10.3791/3424

Lamb, T.D., and E.N. Pugh Jr. 1992. A quantitative account of the activation steps involved in phototransduction in amphibian photoreceptors. *J. Physiol.* 449:719–758. https://doi.org/10.1113/jphysiol.1992.sp019111

Pugh, E.N., Jr, and T.D. Lamb. 1993. Amplification and kinetics of the activation steps in phototransduction. *Biochim. Biophys. Acta.* 1141:111–149. https://doi.org/10.1016/0005-2728(93)90038-H

LaVail, M.M. 1973. Kinetics of rod outer segment renewal in the developing mouse retina. *J. Cell Biol.* 58:650–661. https://doi.org/10.1083/jcb.58.3.650

LeVay, S., T.N. Wiesel, and D.H. Hubel. 1980. The development of ocular dominance columns in normal and visually deprived monkeys. *J. Comp. Neurol.* 191:1–51. https://doi.org/10.1002/cne.901910102

Luo, D.G., and K.W. Yau. 2005. Rod sensitivity of neonatal mouse and rat. *J. Gen. Physiol.* 126:263–269. https://doi.org/10.1085/jgp.200509342

Lyubarsky, A.L., B. Falsini, M.E. Pennesi, P. Valentini, and E.N. Pugh Jr. 1999. UV- and midwave-sensitive cone-driven retinal responses of the mouse: A possible phenotype for coexpression of cone photopigments. *J. Neurosci.* 19:442–455. https://doi.org/10.1523/JNEUROSCI.19-01-00442.1999

Matsumoto, C.S., K. Shinoda, H. Matsumoto, S. Satofuka, A. Mizota, K. Nakatsuka, and Y. Miyake. 2012. Stiles-Crawford effect in focal macular ERGs from macaque monkey. *J. Vis.* 12:6. https://doi.org/10.1167/12.3.6

Meister, M., R.O. Wong, D.A. Baylor, and C.J. Shatz. 1991. Synchronous bursts of action potentials in ganglion cells of the developing mammalian retina. *Science.* 252:939–943. https://doi.org/10.1126/science.2035024

Morgan, J.L., T. Schubert, and R.O. Wong. 2008. Developmental patterning of glutamatergic synapses onto retinal ganglion cells. *Neural Dev.* 3:8. https://doi.org/10.1186/1749-8104-3-8

Murakami, M., and A. Kaneko. 1966. Subcomponents of P3 in cold-blooded vertebrate retinae. *Nature.* 210:103–104. https://doi.org/10.1038/210103a0

Myhr, K.L., P.D. Lukasiewicz, and R.O. Wong. 2001. Mechanisms underlying developmental changes in the firing patterns of ON and OFF retinal ganglion cells during refinement of their central projections. *J. Neurosci.* 21:8664–8671. https://doi.org/10.1523/JNEUROSCI.21-21-08664.2001

Nikonov, S.S., L.L. Daniele, X. Zhu, C.M. Craft, A. Swaroop, and E.N. Pugh Jr. 2005. Photoreceptors of Nrl $^{-/-}$ mice coexpress functional S- and M-cone opsins having distinct inactivation mechanisms. *J. Gen. Physiol.* 125:287–304. https://doi.org/10.1085/jgp.200409208

Nikonov, S.S., R. Kholodenko, J. Lem, and E.N. Pugh Jr. 2006. Physiological features of the S- and M-cone photoreceptors of wild-type mice from single-cell recordings. *J. Gen. Physiol.* 127:359–374. https://doi.org/10.1085/jgp.200609490

Nunn, B.J., J.L. Schnapf, and D.A. Baylor. 1984. Spectral sensitivity of single cones in the retina of *Macaca fascicularis*. *Nature.* 309:264–266. https://doi.org/10.1038/309264a0

Nymark, S., H. Heikkinen, C. Haldin, K. Donner, and A. Koskelainen. 2005. Light responses and light adaptation in rat retinal rods at different temperatures. *J. Physiol.* 567:923–938. https://doi.org/10.1113/jphysiol.2005.090662

Obata, S., and J. Usukura. 1992. Morphogenesis of the photoreceptor outer segment during postnatal development in the mouse (BALB/c) retina. *Cell Tissue Res.* 269:39–48. https://doi.org/10.1007/BF00384724

Okawa, H., and A.P. Sampath. 2007. Optimization of single-photon response transmission at the rod-to-rod bipolar synapse. *Physiology.* 22:279–286. https://doi.org/10.1152/physiol.00007.2007

Olney, J.W. 1968. An electron microscopic study of synapse formation, receptor outer segment development, and other aspects of developing mouse retina. *Invest. Ophthalmol.* 7:250–268.

Pepperberg, D.R., P.K. Brown, M. Lurie, and J.E. Dowling. 1978. Visual pigment and photoreceptor sensitivity in the isolated skate retina. *J. Gen. Physiol.* 71:369–396. https://doi.org/10.1085/jgp.71.4.369

Pepperberg, D.R., M.C. Cornwall, M. Kahlert, K.P. Hofmann, J. Jin, G.J. Jones, and H. Ripps. 1992. Light-dependent delay in the falling phase of the retinal rod photoresponse. *Vis. Neurosci.* 8:9–18. https://doi.org/10.1017/S0952523800006441

Regus-Leidig, H., S. Tom Dieck, D. Specht, L. Meyer, and J.H. Brandstätter. 2009. Early steps in the assembly of photoreceptor ribbon synapses in the mouse retina: The involvement of precursor spheres. *J. Comp. Neurol.* 512:814–824. https://doi.org/10.1002/cne.21915

Renna, J.M., S. Weng, and D.M. Berson. 2011. Light acts through melanopsin to alter retinal waves and segregation of retinogeniculate afferents. *Nat. Neurosci.* 14:827–829. https://doi.org/10.1038/nn.2845

Rich, K.A., Y. Zhan, and J.C. Blanks. 1997. Migration and synaptogenesis of cone photoreceptors in the developing mouse retina. *J. Comp. Neurol.* 388:47–63. https://doi.org/10.1002/(SICI)1096-9861(19971110)388:1<47::AID-CNE4>3.0.CO;2-O

Robson, J.G., and L.J. Frishman. 2014. The rod-driven a-wave of the dark-adapted mammalian electroretinogram. *Prog. Retin. Eye Res.* 39:1–22. https://doi.org/10.1016/j.preteyeres.2013.12.003

Sakurai, K., F. Vinberg, T. Wang, J. Chen, and V.J. Kefalov. 2016. The Na^+/Ca^{2+}, K^+ exchanger 2 modulates mammalian cone phototransduction. *Sci. Rep.* 6:32521. https://doi.org/10.1038/srep32521

Sharma, R.K., T.E. O'Leary, C.M. Fields, and D.A. Johnson. 2003. Development of the outer retina in the mouse. *Brain Res. Dev. Brain Res.* 145:93–105. https://doi.org/10.1016/S0165-3806(03)00217-7

Sosula, L., and P.H. Glow. 1971. Increase in number of synapses in the inner plexiform layer of light deprived rat retinae: Quantitative electron microscopy. *J. Comp. Neurol.* 141:427–451. https://doi.org/10.1002/cne.901410403

Soto, F., X. Ma, J.L. Cecil, B.Q. Vo, S.M. Culican, and D. Kerschensteiner. 2012. Spontaneous activity promotes synapse formation in a cell-type-dependent manner in the developing retina. *J. Neurosci.* 32:5426–5439. https://doi.org/10.1523/JNEUROSCI.0194-12.2012

Stiles, W.S., and B.H. Crawford. 1933. The luminous efficiency of rays entering the eye pupil at different points. *Proc. R. Soc. Lond. - Ser. B Contain. Pap. a Biol. Character.* 112:428–450. https://doi.org/10.1098/rspb.1933.0020

Tian, N., and D.R. Copenhagen. 2003. Visual stimulation is required for refinement of ON and OFF pathways in postnatal retina. *Neuron.* 39:85–96. https://doi.org/10.1016/S0896-6273(03)00389-1

Tian, N., H.P. Xu, and P. Wang. 2015. Dopamine D2 receptors preferentially regulate the development of light responses of the inner retina. *Eur. J. Neurosci.* 41:17–30. https://doi.org/10.1111/ejn.12783

Tikidji-Hamburyan, A., K. Reinhard, R. Storchi, J. Dietter, H. Seitter, K.E. Davis, S. Idrees, M. Mutter, L. Walmsley, R.A. Bedford, et al. 2017. Rods progressively escape saturation to drive visual responses in daylight conditions. *Nat. Commun.* 8:1813. https://doi.org/10.1038/s41467-017-01816-6

Turunen, T.T., and A. Koskelainen. 2017. Transretinal ERG in studying mouse rod phototransduction: Comparison with local ERG across the rod outer segments. *Invest. Ophthalmol. Vis. Sci.* 58:6133–6145. https://doi.org/10.1167/iovs.17-22248

Van Hook, M.J., S. Nawy, and W.B. Thoreson. 2019. Voltage- and calcium-gated ion channels of neurons in the vertebrate retina. *Prog. Retin. Eye Res.* 72:100760. https://doi.org/10.1016/j.preteyeres.2019.05.001

Vinberg, F., and V. Kefalov. 2015. Simultaneous *ex vivo* functional testing of two retinas by *in vivo* electroretinogram system. *J. Vis. Exp.* e52855. https://doi.org/10.3791/52855

Vinberg, F.J., S. Strandman, and A. Koskelainen. 2009. Origin of the fast negative ERG component from isolated aspartate-treated mouse retina. *J Vis.* 9:9.1–9.17. https://doi.org/10.1167/9.12.9

Vinberg, F., A.V. Kolesnikov, and V.J. Kefalov. 2014. Ex vivo ERG analysis of photoreceptors using an in vivo ERG system. *Vis. Res.* 101:108–117. https://doi.org/10.1016/j.visres.2014.06.003

Vinberg, F., T. Wang, A. De Maria, H. Zhao, S. Bassnett, J. Chen, and V.J. Kefalov. 2017. The Na^+/Ca^{2+}, K^+ exchanger NCKX4 is required for efficient cone-mediated vision. *Elife*. 6:e24550. https://doi.org/10.7554/eLife.24550

Vistamehr, S., and N. Tian. 2004. Light deprivation suppresses the light response of inner retina in both young and adult mouse. *Vis. Neurosci.* 21: 23–37. https://doi.org/10.1017/S0952523804041033

Wang, J.S., and V.J. Kefalov. 2011. The cone-specific visual cycle. *Prog. Retin. Eye Res.* 30:115–128. https://doi.org/10.1016/j.preteyeres.2010.11.001

Wong, R.O. 1999. Retinal waves and visual system development. *Annu. Rev. Neurosci.* 22:29–47. https://doi.org/10.1146/annurev.neuro.22.1.29

Yokoyama, S. 2000. Molecular evolution of vertebrate visual pigments. *Prog. Retin. Eye Res.* 19:385–419. https://doi.org/10.1016/S1350-9462(00)00002-1

Zhou, Z.J., and D. Zhao. 2000. Coordinated transitions in neurotransmitter systems for the initiation and propagation of spontaneous retinal waves. *J. Neurosci.* 20:6570–6577. https://doi.org/10.1523/JNEUROSCI.20-17-06570.2000